



## DISSERTATION

# Multi-Electron Dynamics in the Ionization of Molecules by Strong Laser Pulses

ausgeführt zum Zwecke der Erlangung des akademischen Grades eines Doktors der technischen  
Wissenschaften unter der Leitung von

Thomas Brabec

*Center for Photonics Research, University of Ottawa,  
150 Louis Pasteur, Ottawa, ON, K1N 6N5 Canada*

eingereicht an der Technischen Universität Wien  
Fakultät für Elektrotechnik und Informationstechnik  
von

Jürgen Zanghellini

*Matrikelnummer 9525954  
Reschgasse 5/18, A-1120 Wien, Austria, EU*

Wien, im November 2004

DISSERTATION

# Multi-Electron Dynamics in the Ionization of Molecules by Strong Laser Pulses ‡

Jürgen Zanghellini

Center for Photonics Research, University of Ottawa, Ottawa, ON, K1N 6N5  
Canada

E-mail: juergen.zanghellini@tuwien.ac.at

**Abstract.** Shake-up of a two-electron system is investigated in the strong infrared laser field limit, both theoretically and experimentally. During tunnel ionization the electron shakes-up a second electron to an excited bound state. Theoretically, a complete analytical theory of shake-up in intense laser fields is developed. We predict that shake-up produces one excited  $\sigma_u D_2^+$  state in  $\approx 10^5$  ionization events. Shake-up is measured experimentally by using the molecular clock provided by the internuclear motion. The number of measured events is found to be in excellent agreement with theory.

Besides shake-up there are a wealth of multi-electron phenomena in strong laser fields that cannot be treated analytically. Therefore we introduce the multi-configuration time-dependent Hartree-Fock (MCTDHF) method as a new approach towards the numerical solution of the time-dependent Schrödinger equation arising in ultrafast laser dynamics. MCTDHF approximates the exact wave function by several Slater determinants. By doing so the method produces a lower dimensional, non-linear system of coupled differential equations compared to the original Schrödinger equation. MCTDHF is capable of modeling non-perturbative multi-electron dynamics including correlation effects of up to 10 active electrons. We discuss the theoretical foundations of our approach and describe our one dimensional implementation.

To assess the reliability and efficiency of MCTDHF we test the method on two examples, using the harmonic quantum dot and the one-dimensional Helium in strong laser pulses as models. We find rapid convergence for quantities like ground state population, correlation coefficient, and single ionization towards the exact results. The method converges, where time-dependent Hartree-Fock fails qualitatively.

By using one dimensional MCTDHF calculations we then investigate ionization of multi-electron systems. Our analysis reveals the key physical process underlying ionization of complex systems. The laser induced multi-electron dynamics depend on the ratio of laser frequency,  $\omega$ , to plasmon frequency,  $\omega_m$ , discriminating two different regimes. In the over-resonant limit,  $\omega \gg \omega_m$ , tunnel ionization is destroyed. Ionization takes place by a classical over the barrier mechanism. In the under-resonant limit,  $\omega \ll \omega_m$ , tunnel ionization remains dominant, but is weakened by a polarization induced growth of the tunneling barrier.

‡ Parts of this work have been published as

M. Kitzler et al. *Phys. Rev. A*, 70:041401(R), 2004

J. Zanghellini, M. Kitzler, T. Brabec, and A. Scrinzi. *J. Phys. B*, 37:763, 2004

J. Zanghellini et al. *Laser Physics*, 13:1064, 2003

# Contents

---

<b>Contents</b>	<b>iii</b>
<b>Acknowledgments</b>	<b>iv</b>
<b>1 Introduction</b>	<b>1</b>
<b>2 Shake-up excitation during optical tunnel ionization</b>	<b>3</b>
<b>3 The multi-configuration time-dependent Hartree-Fock (MCTDHF) method</b>	<b>10</b>
3.1 The MCTDHF theory	10
3.1.1 Choosing constraints	13
3.1.2 Mean field operator and projector	14
3.2 Understanding MCTDHF	15
3.3 Implementation of the MCTDHF-package	18
3.3.1 One dimensional realization	18
<b>4 Testing the MCTDHF method</b>	<b>23</b>
4.1 The one dimensional harmonic quantum dot	23
4.2 The one dimensional Helium atom	26
<b>5 Ionization dynamics in multi-electron systems</b>	<b>32</b>
<b>6 Conclusions</b>	<b>39</b>
<b>References</b>	<b>41</b>

# Acknowledgments

---

I had help.

For his many insights and his amazing physical intuition, I would like to thank my thoroughly brilliant supervisor Thomas Brabec. While he saw electrons tunneling or electrons getting excited I was just able to spot a multi-dimensional wave function. It is thanks to him that I enjoyed my journey through the quantum wonderland.

In no way less brilliant is Armin Scrinzi, to whom I'm much obliged for showing me how to do scientific work. His merciless comments unerringly revealed several weak points in my original arguments. Beyond being spirited, Armin might be the last sincere theoretical physicist in all of Vienna.

I'd like to unleash my profound gratitude to everyone at the Center for Photonics Research, University of Ottawa, for fruitful discussions and various insights. In particular I'm deeply indebted to my colleagues and friends Markus Kitzler and Christian Jungreuthmayer. Together we managed to overcome the day's exertion as Ph.D. students. Thanks to Christian's *PERL*-scripts I was able to solve problems which I wouldn't have even bothered with otherwise.

I wouldn't have been able to finish this work if it weren't for the love and support of my friends and beloved ones.

# Chapter 1

---

## Introduction

Since the advent of quantum mechanics, a lot of interest has been focused on the dynamics of molecular systems. Over the years many theoretical approaches have been formulated and tested in detail. Interestingly, although the basic equation of quantum mechanics is time-dependent most of these theories concentrate on the time-independent Schrödinger equation using the fact that separation of variables is possible if the Hamiltonian itself is time-independent. In the last two decades, however, the time-dependent formulation has attracted much more interest [1]. Not only is it conceptually simpler, as it requires the solution of an initial value instead of an eigenvalue problem, but the numerical techniques of today are much more efficient than previous methods. Moreover, time-dependent descriptions appeal to one's intuition, simply because experiments are often discussed, both by theorists and experimentalists, in a time-dependent language.

This has been especially true, since a new area in physics has been sparked by newly developed high-power ultrashort laser pulses, with field strengths that exceed the electric field strength in an atom by orders of magnitude, and with time scales that rival electron oscillation periods in atoms and small molecules [2]. Experimental developments - like laser control of the motion of small molecules [3], attosecond pulses [4], and ultrashort electron bunches [5] - increase interest in the dynamics of the electronic hull of atoms and small molecules in strong fields, since tracking of electrons within a few tens of attoseconds ( $10^{-18}$ s) resolution will soon be possible [6]. But theoretical calculations lag behind experimental possibilities in that an exact quantum mechanical solution of the dynamics of multi-electron systems is far beyond reach [7]. As of yet, at most two interacting electrons can be described [8, 9, 10]. These calculations rank among the most demanding tasks of present day high performance computing. The problem becomes clear if one looks at the full solution of the Schrödinger equation of nitrogen for instance. For a fixed nucleus (Born-Oppenheimer approximation) the electronic wave function contains 7 co-ordinates, neglecting spin. Considering only 10 points of the wave function in each of the three spatial directions, would result in  $10^{21}$  numbers. To store this wave function, assuming four bytes per number, one would need  $5.7 \times 10^{12}$  CDs, each with a capacity of 700MB. This incredible amount of data would have to be processed at each time step.

Hence approximate methods are indispensable. Most prominent, we mention the single active electron (SAE) approximation, one of the corner stones of the theory of intense laser matter interaction [11, 12, 13]. It is based on the assumption that only the most weakly bound electron of an atom or molecule interacts with the laser field. The other electrons remain inert. Although this has proven to be a good approximation for atoms and small molecules [14] recent experiments [15, 16] have clearly demonstrated that for the description of more complex systems, such as molecules and clusters, the SAE approximation fails.

Clearly, correlated effects like non-sequential double-ionization [17, 18] cannot be taken into account by the SAE approximation. In the strong field regime non-sequential double-ionization can be understood in terms of the recollision model [19]; an ionized electron quivers in the laser field and can collisionally ionize another electron upon returning to its parent ion. However, for X-ray pulses the mechanism is different. Here, the first electron is ionized by absorbing one X-ray photon and shakes off a second electron on its way out [17, 20]. Thus an interesting question is whether or not shake off is possible in the strong field regime, too. In chapter 2 we address the efficiency of shake off in deuterium in strong laser fields experimentally by measuring the shake off rate and theoretically by utilizing a time-dependent Keldysh-like approach [21].

Unfortunately the applicability of this Keldysh theory is limited. The interaction of strong laser pulses with complex systems requires the handling of both many-body processes and non-perturbative dynamics, each by itself poses difficult theoretical and computational problems. This has spawned great interest in the development of approximate, numerical methods beyond SAE calculations that capture the essential physics and are still computationally feasible. The two main approaches investigated so far are the time-dependent density functional (TDDF) theory [22, 23] and the time-dependent Hartree-Fock (TDHF) method [24, 25, 26, 27, 28, 29]. Both methods do not perform well in describing correlated multi-electron dynamics. Moreover, neither method allows convergence to the exact result, which makes it hard to determine the quality of a calculation. Thus, up to now there has not been a conclusive fully quantum mechanically description of, e.g. the unexpected stability of molecules [15, 16, 30] and small clusters [31] in laser fields. To complicate matters, effects of collective excitation, correlation, screening, or the impact of the external field on internal dynamics have had to be treated in an ad hoc manner.

This motivates our development of a multi-configuration time-dependent Hartree-Fock (MCTDHF) method. It is designed for few ( $\leq 10$ ) electron systems, and allows the systematic inclusion of correlation and explicit inclusion of superposition and excited states. MCTDHF is fully based on first principles and it takes an intermediate position between a full solution of the time-dependent Schrödinger equation (TDSE), which is essentially limited to two-electron systems, and TDDFT, which still is plagued by fundamental problems [32].

We will introduce the MCTDHF method in chapter 3 and provide a detailed overview of its theory. In the course of the discussion we clarify its relation to standard methods and we establish a simple picture of the MCTDHF method. We outline the implementation of our one dimensional (1D) MCTDHF program package<sup>1</sup>.

In chapter 4 we demonstrate the applicability of MCTDHF by comparing its results to (numerically) exact solutions of the TDSE for two 1D examples. Indeed, this test will show that MCTDHF provides a rapid convergence to the exact results, where other methods fail not only quantitatively, but even qualitatively.

In chapter 5 we apply MCTDHF to study the ionization dynamics of model multi-electron systems. We identify the main physical effects determining ionization in multi-electron systems, which we find are molecular size and geometry, electron mobility, and polarizability. In particular, the polarizability adds a correlated multi-electron component to tunnel ionization resulting in a suppression of ionization. Despite the 1D nature of our calculations, reasonable agreement with experiments shows that the essential effects of tunnel ionization are successfully captured by our 1D analysis.

Finally, we conclude this work with a summary of the main issues in chapter 6.

<sup>1</sup> The MCTDHF program package is written in FORTRAN 90 by (in alphabetical order) Jeremie Caillat, Markus Kitzler, Armin Scrinzi, and Jürgen Zanghellini. For further details on the MCTDHF-package, please contact Armin Scrinzi, [armin.scrinzi@tuwien.ac.at](mailto:armin.scrinzi@tuwien.ac.at).

## Chapter 2

---

# Shake-up excitation during optical tunnel ionization

The dominant contribution to non-sequential ionization of atoms in strong laser fields is recollision. The first electron is ionized, accelerated in the laser field, and kicks out a second electron during recollision [33]. The dominant contribution to non-sequential ionization of atoms in X-ray pulses is shake-off. The first electron is ionized by absorbing one X-ray photon and shakes off a second electron on its way out [17, 20].

Little is known about the role of shake-off and shake-up in the strong field regime, although shake-off was originally suggested to be the dominant mechanism in strong field double ionization [18]. In this chapter<sup>1</sup> the gap is closed. Shake-up (SU) in strong laser fields is investigated experimentally and theoretically. Shake-up is used here as the generic term for all excitations generated by the ionizing electron on its way out. SU in atoms and small molecules is expected to be weak. Our analysis is driven by the fact that SU is bound to become prominent in larger molecules, where the energy spacing between ground and excited states becomes small.

Experimentally, we report the first observation of shake-up excitation during strong field ionization. The measurement is done in  $D_2$ . SU creates charged ions at a distance close to the internuclear distance of the neutral molecule. In this way a signature at the high energy end of the kinetic energy spectrum of the ionic fragments is created, from which SU can be identified. A ratio of SU excitation of  $\sigma_u$  to tunnel ionization of  $2 \times 10^{-5}$  is measured in  $D_2$ . Deuterium was chosen for a number of reasons. First, all excited states of  $D_2^+$  are relatively simple and therefore, allow a clean identification of shake-up. Second, as a two-electron system, electron-electron correlation effects can be calculated without too many approximations, facilitating the theoretical analysis.

On the theoretical side, we develop an analytical theory of shake-up in strong laser fields that is in excellent agreement with experiments. The SU excitation process proceeds in two stages referred to as SU1 and SU2 here. In the terminology of x-ray double ionization, SU1 and SU2 correspond to the SU and the two-step one photon (TS1) processes, respectively. SU1: The two-electron wavefunction contains components of all one electron states. Each of these components can lead to tunneling, resulting in regular ionization for the ground state and in shake-up for the excited state component. SU2: On its way out the electron creates an electric dipole field that causes non-adiabatic transitions to excited states. Our theory complements existing theoretical

<sup>1</sup> This chapter has been submitted to *Phys. Rev. Lett.* by the authors I. Litvinyuk, F. Légaré, P. W. Dooley, D. M. Villeneuve, and P. B. Corkum (experiments), as well as J. Zanghellini, A. Pegarkov, C. Fabian, and T. Brabec (theory), 2004.

work on atomic SU1 [34, 35, 36] and determines for the first time the value of the dipole-induced SU2 contribution. SU2 is found to be the dominant mechanism in  $D_2$ .

The theoretical analysis is performed in two steps. SU1 is governed by the part of the wavefunction under the barrier up to the classical birth point at which the electron penetrates the barrier. Tunneling takes place in a fraction of the laser period so that the quasi-static molecular (MO) ADK theory [13, 14] can be applied. SU2 takes place after the electron has been born in the continuum and is calculated using a time dependent, Keldysh-type method [21, 37].

Following MO-ADK [14] we find the ionization rate for SU1 as

$$w_j(t) = \sum_{m'} \frac{B_j^2(m')}{2^{|m'|} |m'|!} \frac{1}{\kappa_j^{2/\kappa_j-1}} \left[ \frac{2\kappa_j^3}{\mathcal{E}(t)} \right]^{2/\kappa_j-|m'|-1} \exp \left[ -\frac{2\kappa_j^3}{3\mathcal{E}(t)} \right], \quad (2.1)$$

where the laser electric field is denoted by  $\mathcal{E}(t)$ ,  $l$  and  $m$  are the angular and magnetic quantum numbers, and  $B_j(m') = \sum_l C_{lj} D_{m'm}^l Q(l, m')$  with  $D_{m'm}^l$  and  $Q(l, m')$  defined in Ref. [14]. The index  $j \in \{0, 1\}$  refers to the ionic  $\sigma_g$  and  $\sigma_u$  states, respectively. The coefficient  $C_{lj}$  is obtained from matching the tunneling wavefunction under the barrier to the corresponding, field free, asymptotic components of  $D_2 \sigma_g$ . We find  $C_{00} = 2.5$  and  $C_{01} = 1.1$ . Terms with  $l > 0$  are negligible for  $D_2$ . Further,  $\kappa_j = \sqrt{2I_{pj}}$ , where  $I_{pj} = (I_g - I_j)$  is the ionization potential of  $D_2$ ,  $I_g$  is the binding energy of the  $D_2 \sigma_g$  state, and  $I_j$  is the binding energy of the  $D_2^+$  states. The difference to conventional ionization is that tunneling depends on the eigen-state the remaining electron ends up after ionization. For  $j = 0$ , the bound electron remains in the ground state and conventional ionization takes place. For  $j = 1$ , the second electron gets bound in the ionic  $\sigma_u$  state. Shake-up results from the fact that the  $D_2$  wavefunction contains components of all single electron bound states, which is a manifestation of its correlated nature. The ionization rates for regular and shake-up ionization are different, as the ionization potential and the coefficient  $C_{lj}$  depend on the final ionic bound state.

The second contribution, SU2, is calculated by a Keldysh-type approach that yields the 2-level equations

$$i \frac{da_0}{dt} = I_0 a_0(t) - \mu F_d(t) a_1(t), \quad (2.2)$$

$$i \frac{da_1}{dt} = I_1 a_1(t) - \mu F_d(t) a_0(t), \quad (2.3)$$

for the  $D_2^+$  molecule in the field of the electron leaving the ion after ionization. Here,  $a_0(t)$  and  $a_1(t)$  are the probability amplitudes of the field free  $\sigma_g$  and  $\sigma_u$   $D_2^+$  states. The term

$$\mu F_d = \frac{\mu \mathbf{x}}{|\mathbf{x}|^3} \quad (2.4)$$

is the dipole contribution to the interaction between tunneling and bound electrons. For the sake of simplicity we assume that the laser electric field and therewith the trajectory of the tunneling electron are parallel to the  $z$ -axis. Then,  $\mu = \mu_0 \cos(\varphi)$  is the dipole component along  $\hat{z}$ ,  $\varphi$  is the angle between  $z$ -axis and molecular axis, and  $\mu_0$  is the dipole moment along the molecular axis. The dipole moment in the plane perpendicular to the molecular axis is zero for homo-nuclear diatomic molecules. The electric field  $F_d = 1/d^2$ , where  $d$  measures the distance of the ionized electron from the center of the molecule. The electron is born at time  $t_0$  at the classical turning point

$$d_0 = \frac{R}{2} \cos(\varphi) + \frac{I_{p0}}{\mathcal{E}(t_0)}, \quad (2.5)$$

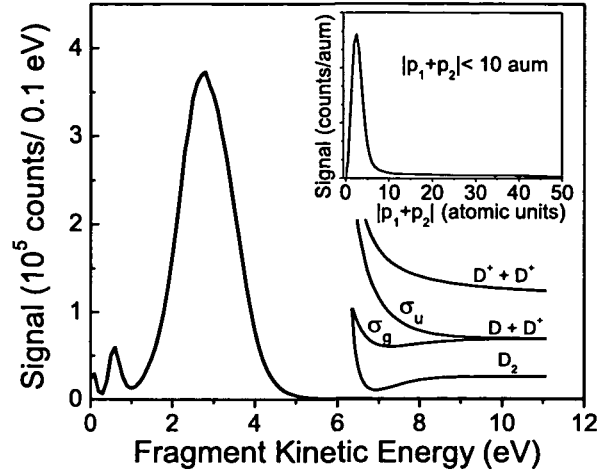


**Figure 2.1.** The main figure shows the measured distribution of correlated  $D^+$  fragments resulting from irradiating  $D_2$  with  $3 \times 10^{14}$  W/cm<sup>2</sup>, circularly polarized light. The upper right figure shows the momentum sum for the two fragments. The pair was considered coincident if the sum was less than 10 atomic units. The potential energy diagram for  $D_2$  is in the lower right. The laser pulse will singly-ionize  $D_2$ , leaving  $D_2^+$  in the  $\sigma_g$  state. Shake-up will leave  $D_2^+$  in the excited  $\sigma_u$  state, resulting in greater kinetic energy release.

and is then accelerated by the laser field following the trajectory

$$d(t) = d_0 + \mathcal{E}(t_0)(t - t_0)^2/2. \quad (2.6)$$

The coupled equations (2.2) and (2.3) are solved by diagonalization. We use the standard transformation [38]

$$(a_0, a_1) = \hat{U}(b_0, b_1) \quad (2.7)$$

where

$$U_{11} = U_{22} = \cos(\xi), \text{ and } U_{21} = -U_{12} = \sin(\xi). \quad (2.8)$$

Further,

$$\xi(t) = -\frac{1}{2} \arctan \left[ \frac{\Omega(t)}{\Delta} \right], \quad (2.9)$$

$$\Omega(t) = 2\mu F_d(t) \quad (2.10)$$

is the Rabi frequency, and  $\Delta = I_1 - I_0$ . Finally,  $b_0, b_1$  are the probability amplitudes of the adiabatic eigenfunctions, dressed by the dipole field  $F_d$  of the escaping electron. Adiabatic means that equations (2.2) and (2.3) are diagonalized and solved exactly in the limit of a time-independent field  $F_d$ . In this limit no shake-up occurs. However, for a time-dependent field, as a result of the time derivative of  $\hat{U}$  in the Schrödinger equation, off-diagonal elements always exist and are responsible for non-adiabatic transitions. SU2 is given by the probability for a

non-adiabatic, dipole-induced excitation times the ionization probability which is

$$v_1(t_0) = w_0(t_0) \left| \int_{t_0}^{\infty} \frac{d\xi}{dt} e^{i\phi(t_0,t)} dt \right|^2, \quad (2.11)$$

with

$$\phi(t_0, t) = \int_{t_0}^t \sqrt{\Delta^2 + \Omega(t')^2} dt'. \quad (2.12)$$

Equation (2.11) presents a general expression for non-adiabatic transitions. SU ionization takes place in the weak field limit,  $\Omega \ll \Delta$ . In this limit, integration of (2.11) yields

$$v_1(t_0) = w_0(t_0) \left| \frac{\mu}{\Delta d_0^2(t_0)} + \frac{\mu}{\Delta \mathcal{E}(t_0) d_0(t_0)} [\Xi(\xi) + \Xi(-\xi)] \right|^2, \quad (2.13)$$

where

$$\Xi(\xi) = \left(1 - \frac{1}{\xi}\right) \exp(\xi) E_1(\xi), \quad (2.14)$$

$$\xi(t_0) = \Delta \sqrt{2d_0(t_0)/\mathcal{E}(t_0)}, \quad (2.15)$$

and

$$E_1(\xi) = \int_{\xi}^{\infty} dt \exp(-t)/t \quad (2.16)$$

is the tabulated exponential integral. For negative  $\xi$  the principal value of  $E_1$  has to be taken.

Our analysis reveals the following intuitive picture of SU2. When the tunneling electron is born at  $t_0$ , the bound electron is in the adiabatic ground state dressed by the dipole electric field, which contains components of the field-free, excited states. However, the population of the field-free excited states is only virtual. In the limit, where the ionized electron is removed infinitely slowly from the ion, the remaining bound electron will make an adiabatic transition from the dipole-field dressed to the dipole-field free ground state, i.e. the bound electron will remain in the ground state. In reality, the ionized electron leaves the nucleus with finite velocity and non-adiabatic transitions take place, which are the source of SU2.

The theory has been tested by experiments relying on the concept of the "molecular clock". First ionization will set in motion a nuclear wave packet on the ground state potential energy surface of  $D_2^+$ . The potential surfaces of  $D_2$  and of its ions are shown in the inset of Fig. 2.1. This motion is well known from theory and experiment [5]. If an electronic excitation were to occur at some later time, the excited molecule would dissociate, with fragment kinetic energy directly reflecting the time delay between ionization and excitation. That allows us to distinguish instantaneous excitation, taking place at the internuclear separation of the neutral molecule, from delayed excitation and ionization, which may happen at later times and larger distances, characteristic of enhanced ionization [39, 40] or re-collision [5]. We assume that the most likely state of  $D_2^+$  to be excited is  $\sigma_u$ , the lowest energy excited state. If the  $\sigma_u$  state is populated at the time of ionization and the molecule dissociates on that potential energy surface, the fragment kinetic energy ( $\approx 9$  eV) will reflect the internuclear separation of the  $D_2$  ground state.

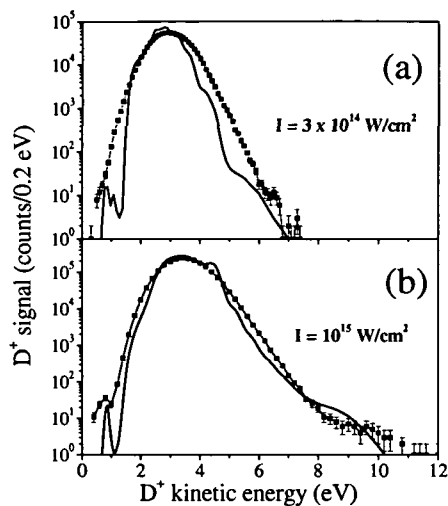


**Figure 2.2.** The dots represent the experimental measurement of kinetic energy release per  $D^+$  fragment, shown with a log scale. The solid curve is the calculation. Two laser intensities are shown. Only for the higher intensity of  $10^{15}$  W/cm<sup>2</sup> is there evidence of shake-up events above 8 eV. The measured branching ratio is  $2 \times 10^{-5}$ .

The extremely low probability of such events would prevent their observation over the noise background if we could only detect a single ion fragment. Fortunately, during dissociation on the  $\sigma_u$  surface of  $D_2^+$  the remaining electron will ionize as the molecule passes the enhanced ionization region. The second ionization step has little influence on the fragment kinetic energy. Most importantly, this process produces a pair of correlated deuterons, which can be detected in coincidence. Conservation of momentum introduces a severe constraint that allows us to dramatically improve the signal to noise ratio for detection of deuterons resulting from double ionization of  $D_2$ . We estimate that such momentum-correlated detection allows us to confidently observe events with relative probability higher than  $10^{-6}$  in respect to single ionization.

The experiment used 40 fs,  $800 \mu\text{J}$  pulses produced by a Ti:sapphire regenerative amplifier operated at 500 Hz. To remove any contribution from re-collision, the pulses were circularly polarized. The pulses were focused inside a vacuum chamber (background pressure  $10^{-9}$  Torr) by an  $f/2$  on-axis parabolic mirror ( $f = 50$  mm) on a beam of deuterium molecules. We estimate our focal spot diameter and confocal parameter to be  $5 \mu\text{m}$  and  $100 \mu\text{m}$ , respectively.

The molecular and laser beams intersected orthogonally inside a uniform acceleration time-of-flight mass spectrometer (240 mm overall length, 200 mm ion flight distance, 70 mm internal diameter) and were mutually perpendicular to the time-of-flight axis. The molecular beam was heavily skimmed such that its width along the laser beam propagation direction was  $40 \mu\text{m}$  FWHM. This ensured that few molecules were outside the high intensity region of the laser focus.

Ions were accelerated by the uniform electric field onto a time- and position-sensitive delay-line anode detector. This detector, in conjunction with a multichannel, multihit time-to-digital

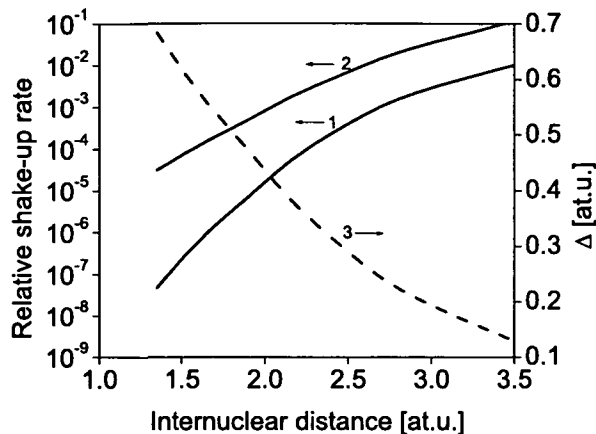


**Figure 2.3.** Relative shake-up rates in  $D_2$  as a function of internuclear distance. Curve 1 (SU1) depicts  $w_1/w_0$ , see equation (2.1). Curve 2 (SU2), depicts  $v_1/w_0$ , see equation (2.13). The rates have been averaged over  $\varphi$ , the angle between laser electric field and molecular axis. Shake-up is calculated at the intensity  $8 \times 10^{14} \text{ W/cm}^2$ . Curve 3 shows  $\Delta$ , the energy difference between the ionic  $\sigma_g$  and  $\sigma_u$  states of  $D_2^+$ .

converter, allowed simultaneous measurement of both ion arrival times (with 500 ps resolution) and positions in the detector plane (with  $250 \mu\text{m}$  resolution) for up to sixteen ion impacts per laser pulse. From the time and position data, the three-dimensional initial velocity vector was computed for each detected ion. The recoil momentum distribution of surviving  $D_2^+$  ions was measured to determine the intensity at which molecules ionized, as described previously [41].

Figure 2.1 represents the kinetic energy distribution of all detected deuterons at  $3 \times 10^{14} \text{ W/cm}^2$  intensity. The enhanced ionization [39, 40] peak at 3 eV per fragment dominates the kinetic energy distribution. The smaller bond softening [42] peak is seen at 0.6 eV. For double-hit events the total (sum) momentum for each deuteron pair was histogrammed (inset to figure 2.1). The peak at low total momentum represents true coincidences, since momentum conservation requires that the momenta of the two deuterons must sum to zero. The high momentum tail of the distribution comes from accidental coincidences, i.e. when deuterons from two different molecules are detected within one event.

The observed width of the true coincidence peak is mainly determined by the width of the ion recoil momentum distribution in circularly polarized light ( $\approx 4 \text{ a.u.}$  of momentum). Additional contributions to the peak width result from the distribution of longitudinal velocities of  $D_2$  in the molecular beam ( $\approx 2 \text{ a.u.}$  of momentum) and the momentum resolution of the detector ( $\approx 1 \text{ a.u.}$  of momentum).

In our analysis we define a correlated double-hit as having a total momentum in the range of 0-10 atomic units of momentum to safely include all possible single molecule events. About 15% of all events were correlated double-hits, reflecting the 50% detection efficiency for the first deuteron and the 30% efficiency of detecting the second fragment. The second deuteron is less likely to be detected due to the dead times of the MCP and anode constant fraction discriminators.

The histograms of kinetic energy (per fragment) of all correlated events at two different laser intensities are shown in figure 2.2. The kinetic energy was calculated in the center-of-mass

frame for each molecule. At  $3 \times 10^{14}$  W/cm<sup>2</sup> [figure 2.2(a)] we observe no correlated events with fragment energies near 9 eV, with the high energy tail of the enhanced ionization peak extending to 7.5 eV. Only a single event with fragment energies above 7.5 eV was observed, and its kinetic energy (14 eV per fragment) was too high to attribute it to D<sub>2</sub> excitation. Thus at this intensity we can impose an upper limit on the probability of instantaneous excitation to be less than  $10^{-6}$ .

However, at  $10^{15}$  W/cm<sup>2</sup> we do see a distinct high energy band at around 9 eV extending beyond the edge of the enhanced ionization peak [figure 2.2(b)]. Though the number of counts is small, it is statistically significant and allows us to estimate the branching ratio between the ground and first excited state of D<sub>2</sub><sup>+</sup> to be about  $2 \times 10^{-5}$ . At this intensity the single ionization of D<sub>2</sub> is saturated and raising the intensity even further would not increase the probability of excitation.

The kinetic energy of the fragments was calculated by solving the nuclear wavepacket propagation on the  $\sigma_g$  and  $\sigma_u$  D<sub>2</sub><sup>+</sup> surfaces [43]. Ionization and shake-up populate the two ionic surfaces according to the rates (2.1) and (2.13). Non-adiabatic population transfer, caused due to the launching of the wavepacket presents a numerical artefact and is filtered. Ionization of D<sub>2</sub><sup>+</sup> is calculated by using numerically determined ionization rates [44]. The numerical results are found to be in excellent agreement with experiment, see figure 2.2.

The excellent agreement between theory and experiment allows us to determine parameter regimes in which SU will make a dominant contribution to non-sequential, correlated ionization. From the inspection of equations (2.1) and (2.13) it becomes clear that SU has to be significant for large molecules, where the energy spacing between the levels becomes small. As a clean measurement in large molecular systems is not straight forward, we suggest the following experiment. The decreasing energy spacing can be emulated by using dissociating or excited vibrational wave packets of diatomic molecules, for which the internuclear distance increases and the energy spacing decreases. In Figure 2.3 SU1 and SU2 are plotted versus internuclear distance of D<sub>2</sub>. At an internuclear distance of 3.5 a.u. the level spacing is  $\approx 3$  eV, which is a typical value found in complex molecules. The ratio of tunneling to SU ionization becomes  $\approx 10^{-1}$ . This reveals the dominant contribution of SU to the ionization of large molecules. SU2 is larger than SU1 over the whole parameter range and therefore presents the leading shake-up mechanism.

## Chapter 3

---

# The multi-configuration time-dependent Hartree-Fock (MCTDHF) method

In this chapter we will introduce the multi-configuration time-dependent Hartree-Fock (MCTDHF) method. Starting with the core approximation of MCTDHF we derive the MCTDHF evolution equations. By comparing MCTDHF to other methods its benefits will become apparent and we will be able to classify MCTDHF with regard to standard methods. This leads to a simple picture in understanding MCTDHF. Finally, we focus on the implementation of the current MCTDHF-program package.

### 3.1 The MCTDHF theory

We are interested in the solution of the time-dependent Schrödinger equation (atomic units are used throughout, unless otherwise stated) in Born-Oppenheimer approximation for an atom or molecule with  $f$  electrons in a time-dependent electric field (typically arising from ultra-short laser pulses),

$$i \frac{\partial \Psi}{\partial t} = H \Psi. \quad (3.1)$$

Here the Hamiltonian,  $H$ , and the electronic wave function  $\Psi = \Psi(\mathbf{x}_1, \dots, \mathbf{x}_f; t)$  are time-dependent. The electron co-ordinates,  $\mathbf{x}_1, \dots, \mathbf{x}_f$ , describe not only the three spatial co-ordinates  $\mathbf{r}_i$  but also the spin co-ordinates  $s_i$ , i.e.  $\mathbf{x}_i = \{\mathbf{r}_i, s_i\}$ .

In MCTDHF one approximates the exact wave function, describing the dynamics of  $f$  electrons, by the ansatz

$$\Psi(\mathbf{x}_1, \dots, \mathbf{x}_f; t) \approx \frac{1}{\sqrt{f!}} \sum_{j_1=1}^n \dots \sum_{j_f=1}^n A_{j_1 \dots j_f}(t) [\varphi_{j_1}(t) \otimes \dots \otimes \varphi_{j_f}(t)](\mathbf{x}_1, \dots, \mathbf{x}_f), \quad (3.2)$$

where both, the linear expansion coefficients  $A_{j_1 \dots j_f}(t)$  and the  $n$  expansion functions  $\varphi_j(\mathbf{x}; t)$ , known as single-particle functions (SPF) or spin orbitals, are time-dependent.

For the following it is convenient to introduce a short-hand notation, where we omit the tensor product sign, i.e.

$$|\varphi_{j_1} \dots \varphi_{j_f}\rangle := |\varphi_{j_1} \otimes \dots \otimes \varphi_{j_f}\rangle. \quad (3.3)$$

As the number of SPF,  $n$ , increases, the wave function gets more accurate. In the limit  $n \rightarrow \infty$  the ansatz is complete. Note that the computational labor, however, increases strongly with  $n$ . Without proof we mention that  $n$  should obey

$$f = 1 \Rightarrow n = 1 \quad \text{and} \quad f \geq 2 \Rightarrow n - f = 2k, \quad k \in \{0, 1, 2, \dots\}, \quad (3.4)$$

otherwise there will be redundant configurations.

The ansatz (3.2) is not unique and therefore requires additional constraints [45],

$$\langle \varphi_i(0) | \varphi_j(0) \rangle = \delta_{ij}, \quad (3.5)$$

$$\langle \varphi_i(t) | \dot{\varphi}_j(t) \rangle = -i \langle \varphi_i(t) | g | \varphi_j(t) \rangle. \quad (3.6)$$

Here  $g$  denotes a Hermitian, but otherwise arbitrary, single particle operator. For simplicity, we usually set  $g \equiv 0$ . However, we will briefly discuss other, nontrivial settings of  $g$  in §3.1.1. We want to point out that the constraint (3.5) together with (3.6) guarantees ortho-normality of the SPF for all times. Finally, it follows from the normalization condition  $\langle \Psi | \Psi \rangle = 1$  that

$$\sum_{j_1=1}^n \dots \sum_{j_f=1}^n |A_{j_1 \dots j_f}|^2 = f! \quad (3.7)$$

Until now we have made no reference to the anti-symmetry of the electronic wave function. As the Hamiltonian and therefore the propagation equations are fully symmetric under exchange of electrons, an initially antisymmetric wave function stays antisymmetric during propagation. It is therefore sufficient to demand that the initial coefficients  $A_{j_1 \dots j_f}$  be fully anti-symmetric with respect to their indices, i.e.

$$A_{j_1 \dots j_k \dots j_l \dots j_f} = -A_{j_1 \dots j_l \dots j_k \dots j_f}. \quad (3.8)$$

This restricts the number of independent expansion coefficients to  $\binom{n}{f}$ . Equivalently we can therefore rewrite (3.2) as

$$|\Psi(t)\rangle = \sum_{1 \leq j_1 < \dots < j_f \leq n} A_{j_1 \dots j_f}(t) |\varphi_{j_1}(t) \wedge \dots \wedge \varphi_{j_f}(t)\rangle, \quad (3.9)$$

where the multi-sum now has to be carried out over all "sorted" multi-index  $(j_1 \dots j_f)$  and

$$|\varphi_{j_1} \wedge \dots \wedge \varphi_{j_f}\rangle = \frac{1}{\sqrt{f!}} \sum_{\mathcal{P}} (-1)^{\mathcal{P}} \mathcal{P} |\varphi_{j_1} \otimes \dots \otimes \varphi_{j_f}\rangle \quad (3.10)$$

denotes the normalized, fully antisymmetric tensor product or Slater determinant. Here  $\mathcal{P}$  is the permutation operator and the summation has to be carried out over all permutations.

Our implementation of MCTDHF is based on the multi-configuration Hartree (no Fock) method of [45], from which it differs in the anti-symmetrization of the electronic wave function. In the subsequent derivation of the MCTDHF evolution equations we therefore closely follow [45].

The time evolution equations for  $A_{j_1 \dots j_f}$  and  $\varphi_j$  are obtained from the Dirac-Frenkel variational principle [46, 47]

$$\langle \delta \Psi | i\partial_t - H | \Psi \rangle = 0. \quad (3.11)$$

Note that it is sufficient to derive the evolution equations for one particle only, since, due to the exchange symmetry, they must be identical for all particles. To derive the equations we will

always single out the "symbolically first" particle. However, as electrons are indistinguishable we will omit a special labeling.

Following [45] we define the single-hole function

$$|\Psi^{(l)}\rangle := \langle \varphi_l | \Psi \rangle = \frac{1}{\sqrt{f!}} \sum_{j_2=1}^n \dots \sum_{j_f=1}^n A_{lj_2 \dots j_f} |\varphi_{j_2} \dots \varphi_{j_f}\rangle, \quad (3.12)$$

which is defined as a linear combination of products of  $f-1$  SPF that do not contain the expansion function for the first co-ordinate. With its help the total wave function may be expressed as

$$|\Psi\rangle = \sum_{l=1}^n |\varphi_l \Psi^{(l)}\rangle. \quad (3.13)$$

Further, we define the matrix of the mean field operator

$$\langle \mathbf{H} \rangle_{j,l} := \langle \Psi^{(j)} | \mathbf{H} | \Psi^{(l)} \rangle, \quad (3.14)$$

the density matrix

$$\rho_{j,l} := \langle \Psi^{(j)} | \Psi^{(l)} \rangle = (f-1)! \sum_{j_2 < \dots < j_f} A_{jj_2 \dots j_f}^* A_{lj_2 \dots j_f}, \quad (3.15)$$

as well as the projector on the space spanned by the SPF

$$\mathbf{P} := \sum_{j=1}^n |\varphi_j\rangle \langle \varphi_j|. \quad (3.16)$$

Performing the variation in (3.11) and using the definitions above, keeping in mind that

$$\sum_{j_1=1}^n \dots \sum_{j_f=1}^n \langle \Psi^{(j)} | \varphi_{j_1} \dots \varphi_{j_f} \rangle \langle \varphi_{j_1} \dots \varphi_{j_f} | = \mathbf{P} \langle \Psi^{(j)} |, \quad (3.17)$$

and

$$\langle \Psi^{(j)} | \mathbf{H} | \Psi \rangle = \sum_{l=1}^n \langle \mathbf{H} \rangle_{j,l} |\varphi_l\rangle, \quad (3.18)$$

one obtains, after rather technical calculations, the non-linear equations [45]

$$i\dot{A}_{j_1 \dots j_f} = \sum_{l_1=1}^n \dots \sum_{l_f=1}^n \langle \varphi_{j_1} \dots \varphi_{j_f} | \mathbf{H} | \varphi_{l_1} \dots \varphi_{l_f} \rangle A_{l_1 \dots l_f} - \sum_{i=1}^f \sum_{l=1}^n g_{j_i, l} A_{lj_1 \dots j_{i-1} j_{i+1} \dots j_f}, \quad (3.19)$$

$$i\dot{\varphi} = \mathbf{g}\mathbf{1}\varphi + (1 - \mathbf{P}) [\rho^{-1} \langle \mathbf{H} \rangle - \mathbf{g}\mathbf{1}] \varphi, \quad (3.20)$$

with  $\varphi = (|\varphi_1\rangle, \dots, |\varphi_n\rangle)^\dagger$  in vector notation,  $\mathbf{1}$  denoting the identity matrix and the matrix element  $g_{j,l} = \langle \varphi_j | \mathbf{g} | \varphi_l \rangle$ .

Again, we emphasize that the MCTDHF evolution equations include the numerically exact results as a limiting case. Let us, for the moment, suppose  $\mathbf{g} \equiv 0$ . Then, for  $n \rightarrow \infty$ , the SPF span the hole space ( $1 - \mathbf{P} = 0$ ) and  $(1 - \mathbf{P})$  in equation (3.20) results in a vanishing

time dependence of  $\varphi$ . The expansion functions become equivalent to the time-independent basis functions of the exact scheme and equation (3.19) reveals the Schrödinger equation. If we suppose  $\varphi$  to be independent of time, i.e.  $\dot{\varphi} = 0$ , even though they may not span the hole space, then (3.19) represents the major scheme used for most of the current time-dependent wave packet propagations. Therein the configurations are fixed and only the expansion coefficients are varied, which corresponds to a full configuration-interaction (CI) approach. Unfortunately in CI-calculations often unmanageable numbers of configurations are required.

In the limit of  $n = f$  one obtains the single-configuration (time-dependent) Hartree-Fock method [28].

Finally, for  $f = 1$  the equations (3.19) and (3.20) 'implode', due to the restriction in equation (3.4), leaving

$$i\dot{A}_1 = \langle \varphi_1 | H | \varphi_1 \rangle A_1, \quad (3.21)$$

$$i|\dot{\varphi}_1\rangle = H|\varphi_1\rangle - |\varphi_1\rangle \langle \varphi_1 | H | \varphi_1 \rangle, \quad (3.22)$$

behind. Formally inserting the former in the latter equation retrieves the exact Schrödinger equation.

Besides the good convergence of MCTDHF, which we will demonstrate in chapter 4, the true power of the method lies in its favorable scaling behavior with the number of electrons. Whereas the storage amount in a straight-forward discretization of the Schrödinger equation with  $P$  grid points increases exponentially with the number of particles  $f$ , i.e.  $P^{3f}$ , MCTDHF grows as

$$\text{memory} \sim \binom{n}{f} + nP^3. \quad (3.23)$$

Here, the first term reflects the growth in the coefficients and the second is given by  $n$  SPF per particle. Note that in any case the evolution equations are three dimensional at the most. Therefore it seems possible to study correlated dynamics of few electron systems with up to 10 electrons without making severe approximations.

### 3.1.1 Choosing constraints

We have derived the MCTDHF evolution equations without explicitly defining the single-particle constraint operator  $g$ . For simplicity, we usually set  $g \equiv 0$ . We want to point out that this, however, does in no means affect the quality of the MCTDHF wave function. For two different but otherwise arbitrary constraint operators  $g$  and  $\tilde{g}$ , respectively, the corresponding sets of evolution equations are connected by a similarity transformation [45]:

$$\tilde{A}_{j_1 \dots j_f} = \sum_{l_1=1}^n \dots \sum_{l_f=1}^n (\mathbf{U}^\dagger)_{j_1, l_1} \dots (\mathbf{U}^\dagger)_{j_f, l_f} A_{l_1 \dots l_f}, \quad (3.24)$$

$$\tilde{\varphi} = \varphi \mathbf{U}, \quad (3.25)$$

with  $\mathbf{U} = \exp[i(\tilde{g} - g)t]$  and  $\tilde{g}_{j,l} = \langle \varphi_j | \tilde{g} | \varphi_l \rangle$ ,  $g$  analog. Thus proofing the independence of the MCTDHF wave function of a specific constraint. Only the numerical effort required for integration of the evolution equations may differ.

For atomic and molecular systems we are concerned with the total Hamiltonian,  $H$ , which may be split into two parts, namely

$$H(\mathbf{x}_1, \dots, \mathbf{x}_f; t) = \sum_{\kappa=1}^f H_1(\mathbf{x}_\kappa; t) + \sum_{\lambda > \kappa}^f H_2(\mathbf{r}_\kappa, \mathbf{r}_\lambda). \quad (3.26)$$

Here  $H_1(\mathbf{x}; t)$  denotes the single-particle part, consisting of operators depending on only a single co-ordinate (including the interaction with the laser pulse), and  $H_2(\mathbf{r}_\kappa, \mathbf{r}_\lambda) = 1/|\mathbf{r}_\kappa - \mathbf{r}_\lambda|$ , the particle-particle interactions. By setting

$$g(\mathbf{x}; t) \equiv H_1(\mathbf{x}; t), \quad (3.27)$$

the constraint operator  $g$  in (3.6) takes the role of a "single-particle Hamiltonian" describing an uncorrelated motion. The evolution equations now read as

$$i\dot{A}_{j_1 \dots j_f} = \sum_{l_1=1}^n \dots \sum_{l_f=1}^n \langle \varphi_{j_1 \dots j_f} | H_2 | \varphi_{l_1 \dots l_f} \rangle A_{l_1 \dots l_f} \quad (3.28)$$

$$i\dot{\varphi} = H_1 \mathbf{1}\varphi + (1 - P)\rho^{-1} \langle H_2 \rangle \varphi. \quad (3.29)$$

We may interpret these equations as an interaction representation of the original scheme: while  $H_1$  stands for the unperturbed Hamiltonian,  $H_2$  defines the perturbation, including all correlation effects. Only the correlational part,  $H_2$ , propagates the coefficients  $A_{j_1 \dots j_f}$ . For disappearing correlation  $A_{j_1 \dots j_f}$  remains constant. Contrary to the discussion for vanishing constraint operator, here, the SPF  $\varphi_i(\mathbf{x}; t)$  are in motion even if the set of expansion functions span the hole space.

The advantage of the interaction formulation is that it allows the usage of numerically favorable split-step methods [48, 49].

### 3.1.2 Mean field operator and projector

In the abstract formulation of the evolution equations (3.20) the computational labor is well hidden in the calculation of the mean field operator  $\langle H \rangle$ ,

$$\begin{aligned} \langle H \rangle_{j,l} &:= \langle \Psi^{(j)} | H | \Psi^{(l)} \rangle, \\ &= \sum_{\kappa=1}^f \langle \Psi^{(j)} | H_1(\mathbf{x}_\kappa; t) | \Psi^{(l)} \rangle + \sum_{\lambda > \kappa}^f \langle \Psi^{(j)} | H_2(\mathbf{r}_\kappa, \mathbf{r}_\lambda) | \Psi^{(l)} \rangle. \end{aligned} \quad (3.30)$$

Here the Hamiltonian,  $H$ , has been split into operators  $H_1$  and  $H_2$ , according to (3.26), acting on one and two particles only, respectively. The single hole function,  $\Psi^{(j)}$ , is given by (3.12).

By changing names of the integration variables and using the anti-symmetry property (3.8), we may simplify (3.30) and obtain

$$\begin{aligned} \langle H \rangle_{j,l} &= \rho_{j,l} H_1(\mathbf{x}_1; t) + (f-1) \sum_{j_2, l_2} \sum_{j_3, l_3} \sum_{j_4, \dots, j_f} A_{jj_2 \dots j_f}^* A_{ll_2 l_3 j_4 \dots j_f} \left[ \langle \varphi_{j_2} | H_2(\mathbf{x}_1, \mathbf{x}_2) | \varphi_{l_2} \rangle_{\mathbf{x}_2} \right. \\ &\quad \left. + \langle \varphi_{j_2} | H_1(\mathbf{x}_2; t) | \varphi_{l_2} \rangle_{\mathbf{x}_2} + \frac{f-2}{2} \langle \varphi_{j_2} \varphi_{j_3} | H_2(\mathbf{x}_1, \mathbf{x}_2) | \varphi_{l_2} \varphi_{l_3} \rangle_{\mathbf{x}_1, \mathbf{x}_2} \right] \end{aligned} \quad (3.31)$$

Here  $\rho$  is the density matrix (3.15), and the index on the brackets indicates integration over the given co-ordinate(s). Since in the above equation the last two terms of the sum in squared brackets are no functions of  $\mathbf{x}_1$  but constant, their effects in the MCTDHF evolution equation (3.20) are annihilated by the projector  $(1 - P)$ . Thus a simplified mean field operator

$$\begin{aligned} \langle H \rangle_{j,l} &= \rho_{j,l} H_1(\mathbf{x}_1; t) + (f-1) \sum_{j_2, l_2} \sum_{j_3, \dots, j_f} A_{jj_2 j_3 \dots j_f}^* A_{ll_2 j_3 \dots j_f} \\ &\quad \times \langle \varphi_{j_2}(t) | H_2(\mathbf{x}_1, \mathbf{x}_2) | \varphi_{l_2}(t) \rangle_{\mathbf{x}_2} \end{aligned} \quad (3.32)$$

may be used, with  $\rho_{j,l} = \sum_{j_2, \dots, j_f} A_{jj_2 \dots j_f}^* A_{lj_2 \dots j_f}$ . The physical meaning of the mean field operator is apparent in the above equation: while the first term is the usual one-particle Schrödinger equation, the second term represents the averaged interaction of one SPF with all others. Adding the suppressed constant terms in (3.32) would only result in an unitary transformation. Note that contrary to standard multi-configuration methods, the matrix of the mean-field operator,  $\langle H \rangle$ , is time-dependent.

The computational labor to evaluate  $\langle H \rangle$  is demanding. To compute the complete density matrix  $\rho$  a (naive) operation count, OC, gives

$$\text{OC}(\rho) \leq n^2 \binom{n-1}{f-1}. \quad (3.33)$$

However, evaluating the interaction term is even more expensive. The sum over  $j_3 \dots j_f$  consists of  $\binom{n}{f-2}$  non-zero elements. For fixed  $j_3 \dots j_f$ ,  $j, j_2$  and  $l, l_2$ , respectively, can assume  $2 \binom{n-f+2}{2}$  values. Therefore, given the function  $\langle \varphi_{j_2} | H_2(\mathbf{x}_1, \mathbf{x}_2) | \varphi_{l_2} \rangle$  on a  $\mathbf{x}_1$  grid with  $P$  points, the total (naive) operation count is

$$\text{OC}(\langle H \rangle) \leq \left[ 2 \binom{n-f+2}{2} \right]^2 \binom{n}{f-2} P \quad (3.34)$$

Note that the naive way of summing leads to an operation count which can easily be intractable: e.g.  $n = 10, f = 8, P = 1000$ , we have  $3 \times 10^7$ . This example illustrates the main bottleneck of the MCTDHF approach: the computation of the mean field operator,  $\langle H \rangle$ . Its evaluation together with the calculation of the projector,  $P$ , requires efficient computation of three dimensional (3D) and 6D integrals. It is therefore mandatory to express  $H_2$  in some kind of multi-pol expansion, thus reducing the operation count drastically. Practicable strategies are currently a main research topic of our group and others. In Ref. [45] a reduction of high-dimensional integrals (here 6D) to lower dimensions (3D) by a product representation is described, which naturally matches the product-expansion of the solution. For the 3D discretization itself, a variety of strategies are being investigated, including discrete variable representations, self-adaptive grids, and ‘‘cascading’’ or ‘‘multilayer’’ techniques as described in Refs. [50, 51]. It is important to notice that the extension to 3D, in principle, only affects the factor functions, whereas the scaling behavior with respect to  $f$  and  $n$  is independent of dimensionality. As yet we have developed a 1D MCTDHF-code, in which the evaluation of the integrals is a minor problem. An outline of the implementation is given in §3.3 or [52].

## 3.2 Understanding MCTDHF

We will demonstrate the meaning of the MCTDHF-ansatz by means of an example, containing two one-dimensional (1D) particles. For simplicity we will not take spin into consideration. Following equation (3.9), MCTDHF makes the ansatz

$$\Psi(\mathbf{x}_1, \mathbf{x}_2; t) = \frac{1}{\sqrt{2}} \sum_{j_1=1}^{n-1} \sum_{j_2 > j_1}^n A_{j_1 j_2}(t) [\varphi_{j_1}(\mathbf{x}_1; t) \varphi_{j_2}(\mathbf{x}_2; t) - \varphi_{j_2}(\mathbf{x}_1; t) \varphi_{j_1}(\mathbf{x}_2; t)]. \quad (3.35)$$

The expression in squared brackets including the normalization constant is called a Slater determinant. Thus MCTDHF consists in approximating the exact wave function as linear combination (weighted by the coefficient  $A_{j_1 j_2}$ ) of different Slater determinants. Apparently, since the expansion coefficients and functions are time-dependent, an additional constraint [equations (3.5) and

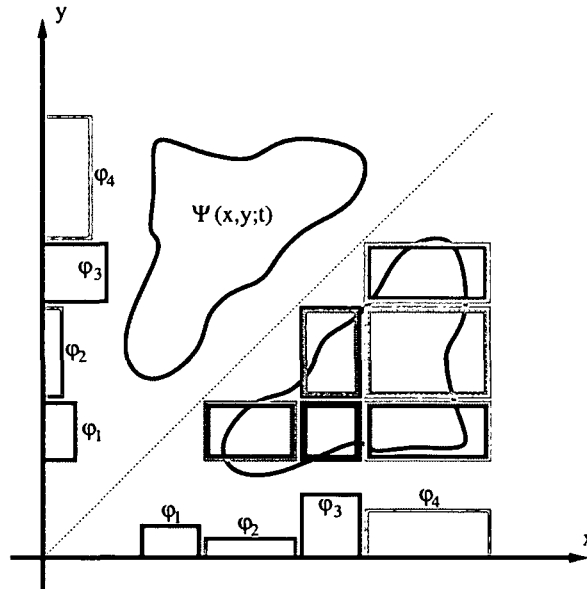


**Figure 3.1.** Approximation of a 2-dimensional, correlated wave function  $\Psi(x_1, x_2; t)$  as a sum of 6 determinants, indicated as rectangular patches. The expansion functions  $\varphi_i$  belonging to their corresponding determinant are drawn along the axes in their respective color.

(3.6)] is needed. Without loss of generality and analog to the usual case of a time-independent expansion, it is most convenient to impose ortho-normality on the expansion functions. The principle of MCTDHF can be seen in figure 3.1. The fully correlated wave function  $\Psi(x_1, x_2; t)$  is approximated by 6 Slater determinants, implying 4 expansion functions per particle. Thus the wave packet is reassembled in a kind of "patch work". Each patch represents one single Slater determinant. Note, however, that the patches do not overlap as a consequence of the imposed orthogonality.

In figure 3.1 we have, for simplicity, assumed the single electron orbitals to be of rectangular shape. However, we emphasize that generally, the expansion orbitals will be a priori unknown. It is important to note that not only the expansion coefficients evolve with time, but the single particle orbital, too. Hence MCTDHF may be interpreted as a truncated configuration-interaction (CI) expansion, in which both, coefficients,  $A_{j_1 j_2}(t)$ , and orbitals,  $\varphi_j(x; t)$ , are optimized. For every time step and fixed number of configuration an optimal expansion is warranted by the variational principle (3.11). Thus resulting in a compact representation of the wave function and hence compressing the necessary storage amount. MCTDHF scales linearly with the number of expansion functions, while the expansion coefficients grow as  $\binom{n}{f}$ . However, it is applicable to more complex systems because already with small configuration numbers (typically  $n - f \in \{4, \dots, 8\}$ ) the "essential physics" is covered, i.e. the number of physically important expansion orbitals, is always much smaller than the number of time-independent basis functions in conventional approaches. Therefore MCTDHF scales more slowly, allowing the treatment of small molecules beyond state of the art 2-electrons-calculation in a numerically converged way. Further, as MCTDHF is a linear combination of different determinants, superpositions and excited states can be

represented inherently.

By increasing the number of configurations MCTDHF allows a systematic inclusion of correlation. It is therefore quite distinct from other theories like the state specific expansion approach (SSEA) [53]. While in the latter it is necessary to identify the major correlation effects and to adjust the approximated expansion accordingly, MCTDHF does not require any a priori knowledge.

These advantages are achieved at the expense of linearity and locality, since the evolution equations in MCTDHF are both, non-linear and non-local. Just as time-dependent Hartree-Fock (TDHF), also MCTDHF with a finite number of configurations suffers, in principle, from the problem of non-linearity of the evolution equations which may lead to a violation of the superposition principle [54]. However, in the case of MCTDHF this problem is greatly reduced, which can be illustrated on the counter-example for TDHF used in [54]: MCTDHF, by construction [equation (3.35)], can describe the superposition of, say, a fractional occupation of the neutral ground state (one configuration) plus a state consisting of a polarized ionic core with one electron far removed (second configuration). This is a situation, where TDHF manifestly fails. Analogously more complex superposition states may require additional configurations, but in the theoretical limit of infinitely many configurations the wave function converges towards the linear time-dependent Schrödinger equation.

In atomic structure theory analyzing multi-configuration wave functions is usually done in terms of the first-order density matrix [55]

$$\gamma_1(\mathbf{x}'_1, \mathbf{x}_1; t) = f \int \Psi(\mathbf{x}'_1, \mathbf{x}_2, \dots, \mathbf{x}_f; t) \Psi^*(\mathbf{x}_1, \dots, \mathbf{x}_f; t) d\mathbf{x}_2 \dots d\mathbf{x}_f. \quad (3.36)$$

The diagonal elements  $\gamma_1(\mathbf{x}, \mathbf{x}; t) d\mathbf{x}$  give the probability for finding a particle within the volume  $d\mathbf{x}$  at the position  $\mathbf{x}$  (including spatial and spin coordinates), while all the other particles have arbitrary positions. In the framework of MCTDHF  $\gamma_1$  is easily computable,

$$\gamma_1(\mathbf{x}'_1, \mathbf{x}_1; t) = \sum_{j,l=1}^n \varphi_l(\mathbf{x}'_1; t) (\tilde{\gamma}_1)_{j,l}(t) \varphi_j^*(\mathbf{x}_1; t), \quad (3.37)$$

$$(\tilde{\gamma}_1)_{j,l}(t) = \sum_{j_2, \dots, j_f} A_{jj_2 \dots j_f}(t) A_{lj_2 \dots j_f}^*(t). \quad (3.38)$$

Thus the matrix  $\tilde{\gamma}_1$  nicely summarizes the many Slater determinants in the wave function in just a few values. Note that  $\tilde{\gamma}_1$  is connected to the MCTDHF density  $\rho$  via transposing.

Of special interest, concerning the interpretation of the MCTDHF wave function, is the case where  $\gamma_1$  and  $\tilde{\gamma}_1$ , respectively, are diagonal. These diagonal elements are known as the natural orbital occupation numbers (NOON) and the respective eigenvectors as natural orbitals (NO) [56]. The NOON values sum up to the total number of particles and can be interpreted as the averaged occupation of each NO. As these orbitals maximize the NOON by diagonalization, it has been shown [56] that NO provide the most rapidly convergent expansion. This is, however, not true for MCTDHF as NO and other SPF span the same space [57]. By choosing the constraint operator accordingly any set SPF can be transformed by a unitary transformation into NO. Nevertheless, NO and NOON in particular provide an important check on the quality of the MCTDHF representation of the wave function, since small natural populations indicate that the MCTDHF expansion is essentially converged.

With regard to an interpretation of multi-configuration wave functions other, equally useful choices of orbitals, are possible. However, for a more thorough discussion we refer to [58].

### 3.3 Implementation of the MCTDHF-package

From a computationally point of view, the most problematic element of the MCTDHF evolution equations is the necessity for a frequent solution of multi-dimensional integrals [equations (3.19) and (3.20)]. Different strategies have been suggested to allow an efficient computation of these integrals [45, 49, 51, 50]. So far, we have successfully implemented a 1 dimensional (1D) version of the MCTDHF method<sup>1</sup>, where these problems are reduced. However, the fundamental difficulty is preserved in the 1D implementation, too. The following explanations may therefore not only be a documentation to the current 1D MCTDHF package, but present a guideline for further expansion of the MCTDHF code to higher dimensions.

#### 3.3.1 One dimensional realization

In the 1D formulation,  $\mathbf{x} = \{r, s\}$ , the MCTDHF evolution equations (3.19) and (3.20) remain unchanged. However, in the current implementation we have chosen to associate the spin part of the electron with the SPF, rather than the co-ordinate, i.e.

$$\langle \mathbf{x} | \varphi_j \rangle = \varphi_j(r, s) \rightarrow \varphi_j(r) \otimes s_j. \quad (3.39)$$

This is meaningful, if we assume that none of the operators mixes spin and spatial space. Hence we neglect any relativistic effects. The general structure of the equations, however, remains unchanged.

For space discretization second order finite differences at equidistant points are used. That is, we use the approximations

$$\frac{\partial \varphi(r)}{\partial r} = \frac{\varphi(r + \Delta r) - \varphi(r - \Delta r)}{2\Delta r} + O[(\Delta r)^2], \quad (3.40)$$

$$\frac{\partial^2 \varphi(r)}{(\partial r)^2} = \frac{\varphi(r + \Delta r) - 2\varphi(r) + \varphi(r - \Delta r)}{(\Delta r)^2} + O[(\Delta r)^2]. \quad (3.41)$$

Integration in space is approximated by simply averaging

$$\int_r^{r+\Delta r} \varphi(r') dr' \approx \frac{\varphi(r) + \varphi(r + \Delta r)}{2} \Delta r. \quad (3.42)$$

The resulting ordinary differential equations in time are solved directly by using a variable order, variable step size explicit Runge-Kutta method. For error estimation in the time integration, extrapolation based on mesh halving is used. A typical (relative) propagation accuracy of  $10^{-8}$  per step was chosen.

For numerical reasons the MCTDHF evolution equations (3.19) and (3.20) have been slightly modified.

Equation (3.20) requires the inversion of the density matrix,  $\rho$ . As the dimension of the density matrix is very small, the numerical effort is negligible. However, problems may arise if the matrix is (almost) singular.  $\rho$  is singular if the population of a natural SPF vanishes. But such an unpopulated state does not contribute to the wave function of the system. To avoid any

<sup>1</sup> The MCTDHF program package is coded in FORTRAN 90, written by (in alphabetical order) Jeremie Caillat, Markus Kitzler, Armin Scrinzi, and Jürgen Zanghellini. If you want to use the MCTDHF-package please contact Armin Scrinzi, [armin.scrinzi@tuwien.ac.at](mailto:armin.scrinzi@tuwien.ac.at)

problems with respect to the inversion we use a regularized form of the original density matrix, i.e.

$$\rho \rightarrow \rho + \varepsilon \mathbf{1}, \quad \varepsilon \ll 1. \quad (3.43)$$

Here  $\varepsilon$  is a number much smaller than unity (typically  $\varepsilon = 10^{-12}$ ) and  $\mathbf{1}$  denotes the unity matrix. Note that such a regularization changes only the time evolution of weakly populated states. Others remain almost unaffected. In our tests the error was below the propagation accuracy.

The ortho-normality relation (3.5) is explicitly enforced after every Runge-Kutta step using the Gram-Schmidt method.

To avoid reflections of outgoing parts of the wave function at the simulation boundaries we artificially change the single-particle Hamiltonian  $H_1(r)$  by adding complex absorbing potentials<sup>2</sup>, CAP( $r$ ) [59], i.e.

$$H_1(r) \rightarrow H_1(r) + i\text{CAP}(r) \quad (3.44)$$

$$\text{CAP}(r) = \begin{cases} 1 - \cos\left(\frac{\pi|x-x_{\text{cap}}|}{2l_{\text{cap}}}\right) & : |x| > x_{\text{cap}} \\ 0 & : \text{else} \end{cases} \quad (3.45)$$

$x_{\text{cap}}$  denotes the point where the CAP is switched on and  $l_{\text{cap}}$  gives the distance to the simulation boundary. Investigations on the dependence on the CAP showed for 'good' (smooth) absorption,  $l_{\text{cap}} > 50$  should be chosen.

We have already pointed out, that the bottleneck of MCTDHF is the evaluation of multi-dimensional integrals. In particular this problem is, in 1D, most pronounced while computing the mean field operator,  $\langle H \rangle$ . In §3.1.2 we have demonstrated that evaluating  $\langle H \rangle$  requires the calculation of integrals of the form  $\langle \varphi_{j_2}(r_2; t) | H_2(r_1, r_2) | \varphi_{l_2}(r_2; t) \rangle$ . Here  $H_2$  denotes the coulombic repulsion of the electrons. By its very nature this interaction is multi-dimensional and non-separable. The MCTDHF algorithm, however, requires the potential to be represented as a linear combination of products of 1D functions. Otherwise the computational labor easily becomes un-doable, see §3.1.2.

### 3.3.1.1 Product expansion of the electron-electron interaction

We seek to approximate the electron-electron interaction,

$$H_2(x, y) = \frac{1}{\sqrt{(x-y)^2 + a^2}}, \quad (3.46)$$

modeled by a "smoothed Coulomb" potential [60], where  $a$  denotes a shielding parameter to avoid singularities, as a sum of products of 1D functions, i.e.

$$H_2(x, y) \approx \sum_{i=1}^m w_i U_i(x) V_i(y), \quad (3.47)$$

where  $m$  is a number ideally much smaller than the number of discretization points,  $P$ , for each SPF  $\varphi_j(x)$ . In the limit  $m = P$ , (3.47) gets exact. The approximation of  $H_2(x, y)$  happens in two steps

<sup>2</sup> CAP are known as negative imaginary potentials (NIP), absorbing boundary conditions (ABC) or optical potentials, too.

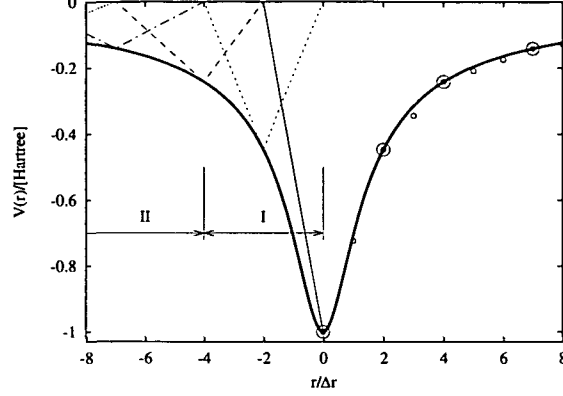


**Figure 3.2.** Approximation of the potential  $\tilde{H}_2(r) = H_2(x-y)$  (thick full line) with "triangular"-shaped expansion functions (thin lines). I and II refer to regions of different width of the expansion functions. Finally the circles mark the discrete and approximated potential,  $\tilde{H}_2^{\text{app}}(r)$  (see text).

- (i)  $H_2(x, y)$  is interpreted as a function  $\tilde{H}_2(r)$  of the single independent variable  $r = x - y$ , sampled at certain points  $r_i, i \in \{1, \dots, m_1\}, m_1 < P$  and approximated linearly in between (similar to a finite element approach). Thus reducing the number of necessary grid points from  $P$  to  $m_1$ .
- (ii) This approximated potential is then factorized by the *Approximationstheorem* of Schmidt [61], leading to the final expansion length  $m$ .

*ad (i)* The operator  $\tilde{H}_2(r)$  is approximated as follows:

$$\tilde{H}_2^{\text{app}}(r) \approx \sum_{i=1}^{m_1} \tilde{H}_2(r_i) \chi_i(r - r_i, \Delta r_i^-, \Delta r_i^+), \quad (3.48)$$

$$\chi_i(r; \Delta r^-, \Delta r^+) = \begin{cases} 1 \pm r/\Delta r^\mp & : \Delta r^\mp > \mp r \geq 0 \\ 0 & : \text{else} \end{cases} \quad (3.49)$$

where  $\Delta r_i^- + \Delta r_i^+$  denotes the "width" of the expansion function  $\chi_i$ . By requiring  $r_{i+1} = r_i + \Delta r_i^+$  and  $\Delta r_{i+1}^- = \Delta r_i^+$  it is guaranteed that in between neighboring sample points,  $r_{i+1}$  and  $r_i$ , two expansion functions are overlapping only. The basic idea of this approximation is to sample not every grid point, for which (3.48) would be exact, but just a few and to approximate the remaining points linearly. This is illustrated in figure 3.2. The potential,  $\tilde{H}_2(r)$ , is sampled with triangular shaped expansion functions (thin lines) given by (3.49), which are weighted by the value of the operator at the sample point (left hand side of figure 3.2). The right hand side of figure 3.2 shows the values of the approximated potential at different grid points. The sample points, for which (3.49) is exact, are marked with big circles, while the points in between are denoted by small circles. The latter quite accurately follow the exact potential (thick line). Note that the distance between the sample points is increasing for increasing  $|r|$  with very little loss of accuracy. This is made possible due to the slow change in  $\tilde{H}_2(r)$  for  $r \rightarrow \infty$ , allowing 'broader' expansion functions  $\chi_i$ . In figure 3.2 the region II marks an area, in which the expansion functions are twice

as "broad" as in region I. The choice of the sample points and sampling intervals is governed by physical reasoning. We will come back to it shortly.

*ad (ii)* The *Approximationstheorem* of Schmidt [61] requires an eigenvalue decomposition of the symmetric positive semi-definite potential density matrix,

$$\Gamma_{j,l} = \sum_{i=1}^{m_1} \tilde{H}_2^{\text{app}}(x_j - y_i) \tilde{H}_2^{\text{app}}(x_l - y_i), \quad (3.50)$$

where  $x_i$  and  $y_i$  denote the  $i$ th grid point,  $1 \leq i \leq m_1$ , of the one-dimensional grid  $x$  and  $y$ , respectively. May  $U_i$  denote the  $i$ th eigenfunction of  $\Gamma$  then the initial potential  $\tilde{H}_2^{\text{app}}(x - y)$  can be expressed as

$$\tilde{H}_2^{\text{app}}(x_j - y_l) \approx \sum_{i=1}^m w_i U_i(x_j) U_i(y_l) \approx H_2(x_j, y_l). \quad (3.51)$$

Note that this expansion, setting  $V_i(y) = U_i(y)$ , is exactly the desired expansion of (3.47). The expansion weights  $w_i$  is given by the overlaps between the potential and the eigenvectors,

$$w_i = \sum_{j=1}^m \sum_{l=1}^m \tilde{H}_2^{\text{app}}(x_j - y_l) U_i(x_j) U_i(y_l) = \pm \sqrt{\lambda_i}, \quad (3.52)$$

where  $\lambda_i$  denotes the  $i$ th eigenvalue of  $\Gamma$ . Since the eigenfunctions are complete over the grid points,  $m_1$ , this expansion is exact for  $m = m_1$ . The representation is proven to be optimal in the  $\mathcal{L}^2$ -sense. That is, the  $\mathcal{L}^2$  error

$$\Delta^2 = \sum_{j=1}^m \sum_{l=1}^m \left[ \tilde{H}_2^{\text{app}}(x_j - y_l) - \sum_{i=1}^m w_i U_i(x_j) U_i(y_l) \right]^2 = \sum_{i=m+1}^{m_1} \lambda_i, \quad (3.53)$$

is minimal [61].

Additionally we control the accuracy of the approximated potential by giving certain regions of space, e.g., small  $|x|$  and  $|y|$ , more weight (implying higher accuracy) than others, since the effect of the electron-electron interaction is negligible if the electrons are far apart. Given the weight function  $\Omega(x, y) > 0$ , equation (3.50) is modified by

$$\tilde{H}_2^{\text{app}}(x, y) \rightarrow \sqrt{\Omega(x, y)} \tilde{H}_2^{\text{app}}(x, y). \quad (3.54)$$

In figure 3.3 we show a representative example of the (relative) error distribution as function of the electron coordinates of the outlined expansion. With only 97 functions  $U_i(x)$  on a  $1000 \times 1000$  grid, one obtains relative accuracies of  $< 1\%$  within a range  $\pm 20$  around the coordinate origin that well exceeds the size of our model atoms and molecules studied subsequently. The approximation fails in the far region for double ionization, where  $|x|$  and  $|y|$  are large simultaneously, describing post-ionization electron momentum distributions for (non-sequential) double ionization incorrectly. However, total double ionization may still be reproduced correctly.

To conclude this chapter, we have presented the MCTDHF method in detail. MCTDHF is a numerically efficient approach to solve the time-dependent many-body Schrödinger equation for

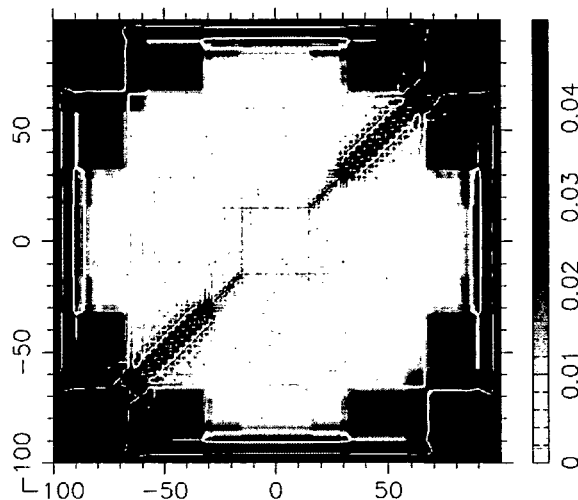


**Figure 3.3.** Relative error distribution of the electron-electron potential expanded as in (3.47) with  $m = 97$  (see text) as function of the electronic co-ordinates (in a.u.). Within a range  $\pm 20$  around the origin of the co-ordinate system the accuracy is better than 1%.

systems of indistinguishable particles ("fermions"). It is fully based on the Dirac-Frenkel variational principle, is thus a formally exact approach, and it is not limited to the perturbation regime. Further, it presents a generalization of the TDHF method. Instead of using a single Slater determinant, in MCTDHF one expands the multi-electron wave function into several determinants, or "configurations". Due to its favourable scaling behaviour compared to standard methods the method allows to go beyond state of the art calculations of 2 electron systems. Therefore it seems possible to study the correlated dynamics of few electron systems with up to 10 electrons without making severe approximations. So far, we have successfully implemented a one-dimensional "toy model" In the following chapter we will assess the reliability and efficiency of the MCTDHF approach and determine the number of configurations needed for convergence based on two examples.

## Chapter 4

---

### Testing the MCTDHF method

The aim of this chapter is to assess the reliability and efficiency of the MCTDHF approach and to determine the number of configurations needed for convergence. This is done by considering two one dimensional (1D) examples, namely the laser driven motion of two electrons in a harmonic oscillator potential and the electron dynamics of a Helium atom irradiated by a short, intense laser pulse. In both cases we solve the time-dependent Schrödinger equation (TDSE, atomic units are used throughout unless otherwise stated)

$$i\Psi(x_1, x_2; t) = H(x_1, x_2; t)\Psi(x_1, x_2; t) \quad (4.1)$$

for a two-electron system with fixed nucleus, described by the Hamiltonian  $H$ , by using the MCTDHF ansatz and comparing with their (numerically) exact counterparts. We investigate quantities like the ground state occupation, correlation coefficient, and single and double ionization, where we find convergence of MCTDHF towards the full TDSE results with a moderate number of configurations. For certain observables like the time evolution of the ground state occupation or double ionization, where TDHF is known to fail, this represents not only a gradual, but a qualitative improvement, while the computational efficiency of TDHF is retained.

#### 4.1 The one dimensional harmonic quantum dot

We first test our approach on the laser driven dynamics of two 1D electrons in a harmonic oscillator potential, for which a semi-analytic solution is available for comparison. The Hamiltonian  $H$  in equation (4.1) for the harmonic quantum dot reads

$$H(x, y; t) = -\frac{1}{2}(\partial_x^2 + \partial_y^2) + \frac{\Omega^2}{2}(x^2 + y^2) + \frac{1}{\sqrt{(x-y)^2 + a^2}} + (x+y)\mathcal{E}_0 \sin(\omega t). \quad (4.2)$$

The interaction between the electrons is modeled by a “smoothed Coulomb” potential [60] with shielding parameter  $a$ . The electrons are coupled to a monochromatic laser field with frequency  $\omega$  and amplitude  $\mathcal{E}_0$ , which is described in dipole approximation and length gauge. Finally,  $\Omega$  denotes the frequency of the harmonic oscillator.

The Hamiltonian (4.2) separates when expressed in new coordinates

$$R = \frac{1}{2}(x+y), \quad \text{and} \quad r = x-y, \quad (4.3)$$

which allows to write the spatial part of the wave function in the factorized form

$$\Psi = e^{-i\epsilon t} \phi(r) \psi(R; t). \quad (4.4)$$

The factors  $\phi(r)$  and  $\psi(R; t)$  are determined by the equations

$$\epsilon \phi(r) = \left( -\partial_r^2 + \frac{\Omega^2 r^2}{4} + \frac{1}{\sqrt{r^2 + a^2}} \right) \phi(r). \quad (4.5)$$

and

$$i\dot{\psi}(R; t) = \left[ -\frac{1}{4} \partial_R^2 + \Omega^2 R^2 - 2R\mathcal{E}_0 \sin(\omega t) \right] \psi(R; t), \quad (4.6)$$

The lowest eigenvalue  $\epsilon$  belongs to an  $x \leftrightarrow y$  exchange symmetric, even function  $\phi(r)$ , i.e. the singlet ground state. While (4.5) can in general only be solved numerically, the solution of the harmonic oscillator problem (4.6) can be given in closed form [62] for an arbitrary initial state wave function  $\psi(R; 0)$ , which we have chosen as the field free ground state.

To determine the correlation of a system we use a measure suggested in [63]. The idea of that measure is based on the existence of an uniquely defined representation of the wave function in terms of single-electron orbitals, for which the single-particle density matrix becomes  $2 \times 2$  block-diagonal. In this canonical representation one writes the wave function as

$$\Psi(x, y; t) = \sum_i p_i(t) \Phi_i(x, y; t), \quad (4.7)$$

where  $\Phi_i$  denotes a Slater determinant consisting of the two single-electron orbitals belonging to the same diagonal block and  $|p_i|^2$  is its occupation probability. Correlation is identified with the number of different determinants  $\Phi_i$  needed to approximate the exact wave function. Normalization of  $\Psi$  requires  $\sum_i |p_i|^2 = 1$ . A ‘‘degree of correlation’’  $K$  is defined as the following measure for the ‘‘length’’ of the sum (4.7)

$$K(t) = \frac{1}{\sum_i |p_i(t)|^4}. \quad (4.8)$$

$K$  does not depend on a specific representation of the wave function, except for choosing the single-electron coordinates  $(x, y)$ . For practical purposes it is useful to note that  $K$  can be calculated without explicit reference to the canonical representation by using the single-particle density operator  $\gamma_1$ , whose kernel is given by

$$\gamma_1(x', x; t) = \int \Psi(x', y; t) \Psi^*(x, y; t) dy. \quad (4.9)$$

The eigenvalues of  $\gamma_1$  are the desired expansion coefficients  $|p_i|^2$ .

For our tests we have chosen  $\Omega = 0.25$  (broad harmonic potentials) and  $a = 0.25$ , where correlation is high ( $K = 1.695$ ). We used a lattice range of  $\pm 10$  with uniform grid spacing of 0.1. The execution time of the program on a 1.8 GHz PC for a typical calculation with 15 configurations was less than 1 hour.

Table 4.1 lists the ground state energy  $E_\eta$  of the system together with the degree of correlation  $K_\eta$  as a function of the number  $\eta$  of MCTDHF configurations. In contrast to real atomic and molecular systems, the ground state energy of the harmonic oscillator is strongly modified by correlation. The correlation energy, i.e. the difference between single configuration Hartree-Fock and the exact energy is  $E_1 - E = 0.3547$ . For 15 configurations the overlap  $|\langle \Psi_{15} | \Psi_\infty \rangle|^2$  between

**Table 4.1.** Initial energy  $E_\eta$  and degree of correlation  $K_\eta$  for an increasing number of configurations  $\eta$ .  $\eta = \infty$  refers to the exact values.

$n$	$\eta = \binom{n}{2}$	$E_\eta$	$\frac{E_\eta - E_\infty}{E_\infty}$	$K_\eta$	$\frac{K_\eta - K_\infty}{K_\infty}$
2	1	1.1795	0.4301	1.0000	-0.4100
4	6	1.0214	0.2384	1.3568	-0.1996
6	15	0.8261	0.0016	1.7260	0.0181
8	28	0.8255	0.0009	1.7150	0.0117
10	45	0.8250	0.0002	1.7029	0.0045
12	66	0.8249	0.0001	1.6998	0.0027
$\infty$	$\infty$	0.8247	0.0000	1.6951	0.0000

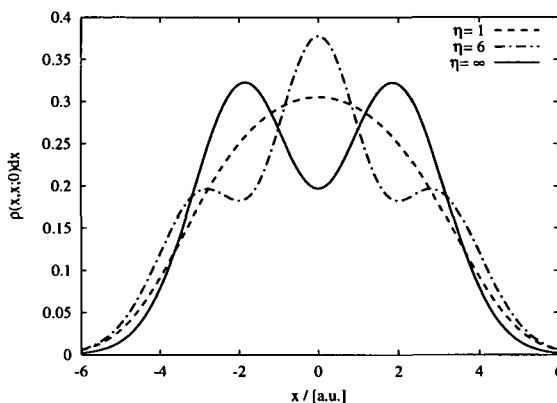


**Figure 4.1.** Electron density  $\rho(x, x; 0)$  for the ground state wave function and an increasing number of configurations  $\eta$ . ( $\eta = \infty$  refers to the numerically exact solution.) The result for  $\eta = 15$  coincides with the exact result within the resolution of the plot.

the MCTDHF and the exact ground state wave function is 0.99939. Convergence beyond that value is rather slow with an overlap of 0.99989 for 66 configurations. It is interesting to note that  $K_\eta$  does not increase monotonically with  $\eta$ . This indicates that with fewer configurations the populations  $|p_i|^2$  may be more evenly distributed for the variationally optimal energy  $E_\eta$  than for a large number of configurations.

The ground state electron density distribution calculated by MCTDHF is plotted in figure 4.1 for various numbers of configurations. Good agreement is achieved for more than 6 configurations. Note that in the correct result the electrons tend to accumulate at two separate maxima, which differs qualitatively from the TDHF electron density with a single maximum at the center.

Next we investigate the time-evolution of our system. We find that correlation,  $K$ , varies only weakly during the evolution, not exceeding the level  $\lesssim 10^{-5}$  even at field strength  $\mathcal{E}_0 = 1$ . We use the overlap of the time-dependent wave function with the ground state  $|\langle \Psi(x, y; 0) | \Psi(x, y; t) \rangle|^2$  to monitor the convergence of the dynamical behavior of the system. Figure 4.2 shows the overlap

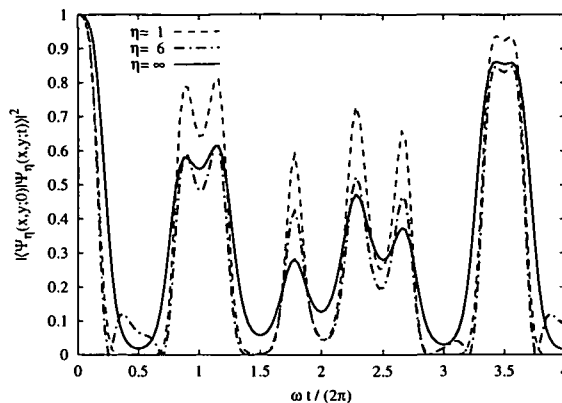


**Figure 4.2.** Probability of being in the ground state  $|\langle \Psi_\eta(x, y; 0) | \Psi_\eta(x, y; t) \rangle|^2$  for an increasing number of configurations  $\eta$  ( $\eta = \infty$  refers to the numerically exact solution) in the presence of an electric field of strength  $\mathcal{E}_0 = 1$  and frequency  $\omega = 8\Omega$ . The result for  $\eta = 15$  coincides with the exact result within the resolution of the plot.

for the parameters  $\mathcal{E}_0 = 1$  and  $\omega = 8\Omega$ . In single-configuration one sees significant deviations from the exact result. At times, the probability is overestimated and, more importantly, at other times it is reduced to almost 0. With 6 configurations the probability curve changes significantly giving a first estimate of the error of the single-configuration Hartree-Fock. Already the curve with 15 configurations coincides with the exact calculation within a maximal absolute error of 0.004582, which may be considered satisfactory accuracy.

## 4.2 The one dimensional Helium atom

The Helium atom is known to be one of the most strongly correlated atomic systems and serves as the basic testing ground for multi-electron calculations. Here we use a 1-dimensional Helium model to investigate the performance of MCTDHF in describing single and double ionization.

The total time-dependent Hamiltonian  $H$  in equation (4.1) for our 1D Helium atom irradiated by a laser field  $\mathcal{E}(t)$  reads

$$H(x, y; t) = -\frac{1}{2}(\partial_x^2 + \partial_y^2) - \frac{2}{\sqrt{x^2 + b^2}} - \frac{2}{\sqrt{y^2 + b^2}} + \frac{1}{\sqrt{(x-y)^2 + b^2}} + (x+y)\mathcal{E}(t), \quad (4.10)$$

where the electron-electron interaction and the electron-nucleus interaction are modeled by the usual “smoothed Coulomb” potential with shielding parameter  $b$ . We set  $b = 0.7408$  and solved the TDSE numerically on the full 1+1 dimensional grid and by MCTDHF on the corresponding 1-dimensional grid. The lattice range is chosen to  $\pm 200$  with a uniform grid spacing of 0.2. Propagating the field-free Hamiltonian in imaginary time results in a singlet ground state energy of  $E_0 = -2.9022$ , which approximates the 3D ground state energy of 3D Helium.

Table 4.2 lists the ground state energy  $E_{0,\eta}$  of our Helium model together with the degree of correlation  $K_\eta(0)$  as a function of the number  $\eta$  of MCTDHF configurations. Both values vary only little with the number of configurations. As in the case of the harmonic quantum

**Table 4.2.** Ground state energy  $E_{0,\eta}$  and degree of correlation  $K_\eta(0)$  for an increasing number of configurations  $\eta$  for the 1D helium atom.  $\eta = \infty$  refers to the numerically exact values.

$n$	$\eta = \binom{n}{2}$	$E_{0,\eta}$	$\frac{E_{0,\eta} - E_{0,\infty}}{E_{0,\infty}}$	$K_\eta(0)$	$\frac{K_\eta(0) - K_\infty(0)}{K_\infty(0)}$
2	1	-2.8830	$-6.62 \times 10^{-3}$	1.00000	$-1.66 \times 10^{-2}$
4	6	-2.8993	$-9.91 \times 10^{-4}$	1.01598	$-8.98 \times 10^{-4}$
6	15	-2.9019	$-1.07 \times 10^{-4}$	1.01684	$-5.38 \times 10^{-5}$
8	28	-2.9022	$-3.10 \times 10^{-5}$	1.01690	$7.92 \times 10^{-6}$
10	45	-2.9022	$-6.17 \times 10^{-6}$	1.01690	$6.00 \times 10^{-6}$
12	66	-2.9022	$-2.17 \times 10^{-6}$	1.01690	$3.23 \times 10^{-6}$
$\infty$	$\infty$	-2.9022	0.00	1.01690	0.00

dot, they converge towards the exact values with increasing number of configurations. While correlation has a relatively little effect on the total energy, it strongly modifies the wave function at larger distances, where it produces noticeable pinches in the probability density along the diagonal  $x = y$ . This is shown in figure 4.3, where logarithmic contour maps of the ground state probability density for various number of configurations are plotted. It is well known that a single configuration calculation does not reproduce those bumps, but with increasing configurations the structures are recovered. This can be quantified by the overlap: With  $\eta = 15$  configurations  $|\langle \Psi_{15}(x, y; 0) | \Psi_\infty(x, y; 0) \rangle|^2 = 0.99994$ , where  $\Psi_\infty$  denotes the numerically exact solution. For  $\eta = 45$  the agreement is excellent, overlapping the exact wave function to 99.999%.

In order to analyze the dynamic quality of our approach the Helium model is irradiated by a short, intense, linearly polarized laser pulse with frequency  $\omega = 0.1837$  a.u. (wavelength  $\lambda = 248$  nm) and peak amplitude  $\mathcal{E}_0 = 0.1894$  a.u. (peak intensity  $I = 1.26 \times 10^{15}$  W/cm<sup>2</sup>). Thus the laser field has the form

$$\mathcal{E}(t) = \mathcal{E}_0 f(t) \sin(\omega t), \tag{4.11}$$

where the envelope  $f(t)$  is chosen to be trapezoidal, with 2-cycle turn-on and turn-off and a 2-cycle flat top.

To investigate the dynamic properties we show logarithmic contour maps of the probability density at the end of the laser pulse for various configurations (figure 4.4). All sub-figures are dominated by probability flows along the  $x$  and  $y$  axis, indicating single-ionization, but differ in their distribution off the axes, representing double-ionization. While Hartree-Fock fails completely to account for double-ionization, higher configuration calculations do exhibit two-electron detachment. None of the tested configurations shows the pronounced avoidance of the wave function along the potential ridge ( $x = y$ ), which is a known artefact of TDHF methods [24, 29]. MCTDHF still does not correctly reproduce two-electron distributions, but total double ionization is well reproduced, as will be demonstrated below.

We now turn to a more quantitative investigation of the ionization process. To this end we define various multi-photon absorption probabilities [29, 64] and calculate them at the end of the laser pulse at time  $t = 6T_L$ , where  $T_L = 2\pi/\omega$  denotes the cycle duration of the laser. The probability of being in the ground state is estimated by

$$P^0 = |\langle \Psi(x, y; 0) | \Psi(x, y; 6T_L) \rangle|^2. \tag{4.12}$$

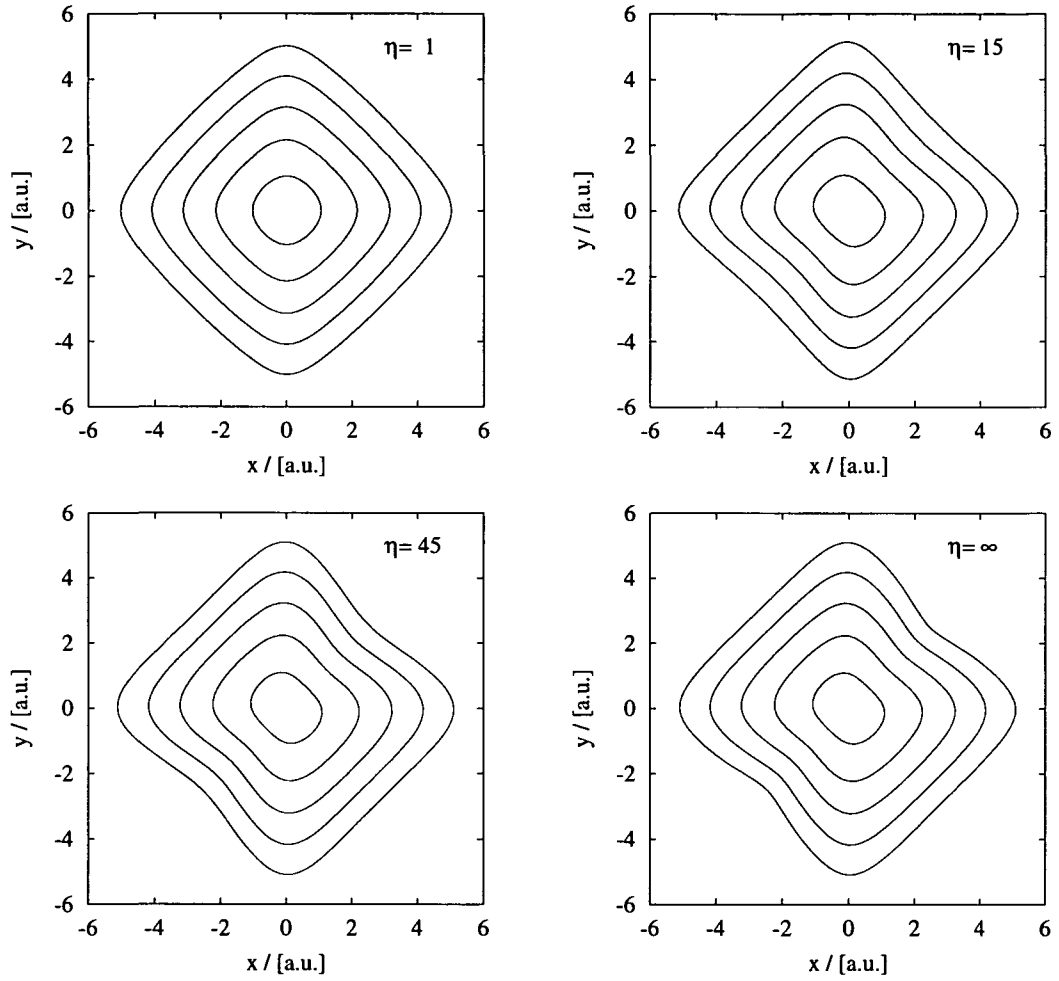


**Figure 4.3.** Logarithmic contour maps of the ground state probability density of Helium for various configurations  $\eta$ . ( $\eta = \infty$  refers to the numerically exact solution.) Contours differ by a factor of 10, representing 0.1 for the innermost line.

For an estimate of total bound state population after the pulse we replace the (unknown) excited two-electron bound states of the system by products of single-electron bound states. Let  $\phi_i$  denote a complete set of field-free bound states for the atomic ion. The probability of finding two electrons in bound states is then estimated as

$$\sum_{i,j} P_{i,j} = \sum_{i,j} |\langle \phi_i(x)\phi_j(y) | \Psi(x, y; 6T_L) \rangle|^2. \quad (4.13)$$

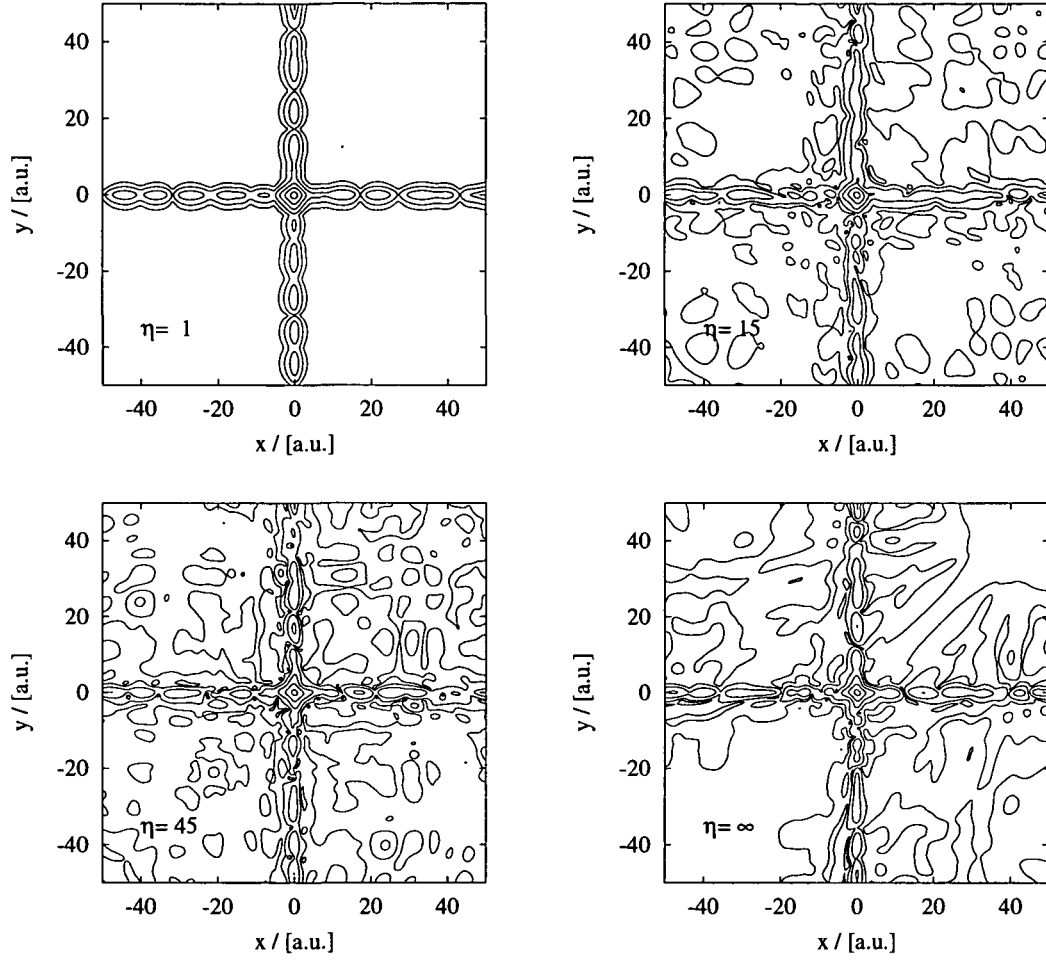


**Figure 4.4.** Logarithmic contour maps of the probability density of Helium at the end of the laser pulse (peak intensity  $I = 1.26 \times 10^{15} \text{W/cm}^2$ ) for various configurations  $\eta$ . ( $\eta = \infty$  refers to the numerically exact solution.) Contours differ by a factor of 10.

The probability  $P^+$  of single-ionization is calculated as

$$P^+ = 2 \sum_i \left[ \int dx |\langle \phi_i(y) | \Psi(x, y; 6T_L) \rangle|^2 - \sum_j P_{i,j} \right], \quad (4.14)$$

while the double ionization probability  $P^{2+}$  is given by

$$P^{2+} = 1 - P^+ - \sum_{i,j} P_{i,j}. \quad (4.15)$$

**Table 4.3.** Probability of total ionization  $P^{tot}$  of a 1D Helium atom at different intensities for an increasing number of configurations  $\eta$ .  $\eta = \infty$  refers to the numerically exact values.

$n$	$\eta = \binom{n}{2}$	$I = 1.26 \cdot 10^{15} \text{W/cm}^2$		$I = 5.00 \cdot 10^{15} \text{W/cm}^2$	
		$P_{\eta}^{tot}$	$\frac{P_{\eta}^{tot} - P_{\infty}^{tot}}{P_{\infty}^{tot}}$	$P_{\eta}^{tot}$	$\frac{P_{\eta}^{tot} - P_{\infty}^{tot}}{P_{\infty}^{tot}}$
2	1	0.1548	-0.4120	0.7936	-0.0978
4	6	0.2210	-0.1606	0.8474	-0.0367
6	15	0.2241	-0.1488	0.8265	-0.0604
8	28	0.2476	-0.0596	0.8323	-0.0538
10	45	0.2485	-0.0565	0.8325	-0.0536
12	66	0.2555	-0.0296	0.8388	-0.0464
$\infty$	$\infty$	0.2633	0.0000	0.8797	0.0000

**Table 4.4.** Multi-photon ionization of a 1D Helium atom at an intensity of  $I = 1.26 \times 10^{15} \text{W/cm}^2$  for an increasing number of configurations  $\eta$ .  $\eta = \infty$  refers to the numerically exact values.

$n$	$\eta = \binom{n}{2}$	$P_{\eta}^0$	$\frac{P_{\eta}^0 - P_{\infty}^0}{P_{\infty}^0}$	$P_{\eta}^+$	$\frac{P_{\eta}^+ - P_{\infty}^+}{P_{\infty}^+}$	$P_{\eta}^{2+}$	$\frac{P_{\eta}^{2+} - P_{\infty}^{2+}}{P_{\infty}^{2+}}$
2	1	0.8923	0.1032	0.1488	-0.3734	0.0059	-0.7859
4	6	0.8533	0.0550	0.1963	-0.1734	0.0246	-0.0428
6	15	0.8308	0.0272	0.2051	-0.1364	0.0189	-0.2645
8	28	0.8264	0.0217	0.2225	-0.0631	0.0250	-0.0272
10	45	0.8188	0.0123	0.2201	-0.0732	0.0283	0.1011
12	66	0.8129	0.0050	0.2281	-0.0395	0.0273	0.0622
$\infty$	$\infty$	0.8088	0.0000	0.2375	0.0000	0.0257	0.0000

Finally we get the total ionization probability

$$P^{tot} = P^+ + P^{2+}. \tag{4.16}$$

Table 4.3 lists the total ionization probabilities depending on the number of MCTDHF configurations  $\eta$  for two different intensities. We first note, that at both intensities ionization is underestimated. Further table 4.3 confirms the insufficiency of TDHF. Including more configurations does significantly reduce the error, resulting in errors of roughly 5% for  $\eta \geq 28$ . A further reduction of the error is possible, but with soaring costs.

At an intensity of  $I = 1.26 \times 10^{15} \text{W/cm}^2$  significant double ionization takes place as can be seen in table 4.4, where the multi-photon ionization probabilities are listed. As figure 4.4 implies, the TDHF approximation fails completely to describe double-ionization, but higher configurations do agree on predicting double-ionization probabilities of about 2.5%. Already with 6 configurations one can account for the essential physics, predicting a 4 times higher double ionization probability as TDHF. Convergence to results better than that needs a large number of configurations making the calculation computationally expensive.

Summing up we have demonstrated that by systematic inclusion of correlation the MCTDHF method provides a good approximation of time-dependent multi-electron wave functions. We have tested our approach on two highly correlated two electron systems. For bound states dynamics MCTDHF provides a rapidly convergent expansion. For ionizing systems MCTDHF is capable of describing the strongly correlated process of double ionization correctly. A quantitative description of single and double ionization within an accuracy of 5% can be achieved with reasonable number of configurations. We have detected no artefacts of the method as they were reported about time-dependent density functional theory [32]. The demonstrated convergence behavior and moderate increase of problem size with the number of electrons makes MCTDHF a powerful approach for the calculation of the correlated dynamics of many electron systems in strong fields, where calculations with up to 10 active electrons and a significant amount of correlation may be feasible.

## Chapter 5

---

### Ionization dynamics in multi-electron systems

The interaction of intense laser fields with matter results in optical field ionization. An exact quantum mechanical treatment of this process is beyond current computer capabilities [7]. However, in noble gas atoms [65, 13] and in small molecules [66, 14] theories based on the single active electron (SAE) approximation excellently describe experimental findings. The SAE approximation rests upon the assumption that only the weakest bound electron interacts with the laser field. However, non-sequential ionization of atoms [18, 67] and recent experiments as the unexpected stability of larger molecules against ionization [68, 15, 30, 69] clearly reveal the multi-electron nature of strong laser field-matter interaction. To identify the corresponding effects - at least in principle - we present a 1D MCTDHF analysis of ionization of complex, extended systems.

Both, single- and multi-electron phenomena play an important role in complex materials. As both effects are closely intertwined, it is helpful to investigate them separately. Therefore, this chapter is organized in the following way. The first part of it is devoted to the investigation of single electron effects in complex systems. Whereas in the second part the analysis is generalized to the multi-electron case.

In the following, we perform calculations for  $f = 1$ ,  $n = 1$ , and  $f \in \{2, 4\}$ ,  $n = 8$  as well as  $f = 6$ ,  $n = 12$ . In the multi-electron case, a further increase of  $n$  changes the ionization yield by less than  $\pm 1\%$  indicating convergence to the exact multi-dimensional wavefunction. The Schrödinger equation is solved on a 1D-grid with a uniform grid spacing of 0.15 and 4000 grid points. To avoid reflection at the simulation boundaries, complex absorbing potentials are used. The ground-state wavefunction is found by propagating the field free Hamiltonian in imaginary time. For details of the numerical technique see [52].

We investigate the ionization yield of a single electron in a square well potential with ionization potential,  $I_p = 0.25$ , depending on the well width  $L$ .  $I_p$  is kept constant by adjusting the well depth  $D$  accordingly. The total Hamiltonian reads

$$H(x; t) = \frac{1}{2} \left[ i\partial_x + \frac{\mathcal{A}(t)}{c} \right]^2 - D \exp \left[ - \left( \frac{2|x|}{L} \right)^{10} \right]. \quad (5.1)$$

Here  $c$  denotes the speed of light and  $\mathcal{A}$  the vector potential of the laser. The laser field has the form  $\mathcal{E}(t) = -\dot{\mathcal{A}}(t) = \mathcal{E}_0 f(t) \cos(\omega t)$ , with peak amplitude  $\mathcal{E}_0 = 0.038$ , frequency  $\omega = 0.057$  and Gaussian envelope  $f(t)$ , duration 10fs FWHM. To numerically model the square well, a super-gauss (exponent 10) is used.

Figure 5.1 shows the ionization yield of a single electron in a square well versus its width. The first feature is the sharp rise of the ionization probability for modest well widths,  $L < 10$ ,

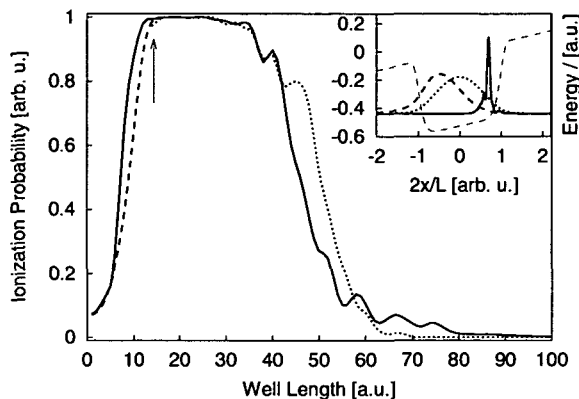


**Figure 5.1.** Ionization probability of a single electron in a square well potential versus its width,  $b$ , calculated quantum mechanically (full line), analytically [equations (5.2) and (5.3), dashed line], and classically (dotted line). The ionization potential,  $I_p = 0.25$ , is kept constant by adjusting the well depth accordingly. The system was exposed to a 800 nm, Gaussian laser pulse of duration 10 fs FWHM and peak electric field strength,  $\mathcal{E}_0 = 10^{13} \text{ Wcm}^{-2}$ . The arrow indicates the case where the transition frequency from ground and first excited state equals the laser frequency.

which is in contradiction to atomic ionization theory. Following atomic ionization theory, the Keldysh parameter [65],  $\gamma = \omega\kappa/\mathcal{E}_0$ , with  $\kappa = \sqrt{2I_p}$ , indicates that for our parameters ( $\gamma = 0.34$ ) ionization is to occur predominantly via tunneling. But atomic tunnel ionization theory depends on  $\kappa$  and  $\mathcal{E}_0$  only [13], predicting an ionization probability independent of  $L$ , since the atom essentially is modeled as zero-range potential. A correction to atomic tunnel ionization theory has been developed to account for molecular extension and was successfully applied to small hydrocarbon molecules [70]. It was, however, interpreted differently. We therefore calculate the tunnel ionization rate for a square well potential following [13], which yields

$$w(t) = c(L)\kappa^2 \exp\left[-\frac{2\kappa^3}{3\mathcal{E}(t)}\right] \quad (5.2)$$

$$c(L) = \frac{\cos^2(kL/2) \exp(\kappa L)}{\cos^2(kL/2) - \kappa L/2 + (\kappa/2k) \sin(kL)}. \quad (5.3)$$

Here,  $k = \sqrt{2(D - I_p)}$ , and the structural correction factor,  $c$ , is determined by the magnitude of the absolute squared of the asymptotic ground-state wavefunction in the classically non-allowed region. In the limit of  $L \rightarrow 0$ ,  $D \rightarrow -\infty$ , the parameter  $c \rightarrow 1$ , and the tunneling rate of a 1D delta-function potential is recovered. It follows from equation (5.3), that with increasing system width a larger portion of the ground state wave function is pushed into the classically non-allowed region. Thus increasing the ionization rate. In fig. 5.1 we have compared the numerical and analytical ionization yield. For  $L \leq 6$  the agreement is excellent. Note that equation (5.3) depends exponentially on  $L$ , hence explaining the sharp rise of the ionization yield.

For larger  $L$  ( $6 < L \leq 13$ ) the numerical and analytical ionization yield differ by a factor of up to 2. This difference arises due to the increased density of bound states for larger well widths. Thus the electron mobility picks up, too, and the electron is pushed adiabatically towards the

tunneling barrier. As a result, the wavefunction under the barrier increases, and ionization is enhanced. This effect is not included in the analytical expression (5.3), since Keldysh theory deals with the motion of the electron under the potential barrier only, and ignores the dynamics inside the well [15]. For values  $L > 13$  equation (5.2) loses its validity, since this regime is characterized by the onset of barrier suppression, leaving the system totally ionized.

It therefore surprises that for large  $L > 25$  the ionization yield drops, as it is shown in figure 5.1. Further, for  $L > 80$  ionization is completely inhibited. Since the transition frequency  $\Omega_{01}$  between ground and first excited state is rather small ( $\Omega_{01} < 0.05$ ), the density of bound states is extremely large. Thus the mobility of the electron is high, too, and its dynamic is close to the motion of a free electron. A free electron moves  $180^\circ$  out of phase with the electric laser field strength. Thus, contrary to the case of  $L < 13$ , the electron is pulled away from the tunneling barrier, hence suppressing tunneling ionization. This is illustrated by the inset of figure 5.1. There we show the electron probability distribution at the peak of the laser pulse for  $L = 10$  (dashed line) and  $L = 55$  (full line). The response of the electron is similar to the motion of electrons in over-resonantly driven oscillators [71].

Our calculations identify two regimes of laser-matter interaction, which are governed by the relation of  $\omega$  to  $\Omega_{01}$ . The arrow in figure 5.1 denotes the case of  $\Omega_{01} = \omega$ . As  $\Omega_{01}$  decreases with increasing well length, the area left and right to the arrow present the under- ( $\Omega_{01} > \omega$ ) and the over-resonant ( $\Omega_{01} < \omega$ ) limit, respectively. While the under-resonant regime is accessible via quantum mechanics only, the over-resonant case is dominated by the driving force, allowing a classical description, too.

As the wavefunction is pushed away from the tunneling barrier, one would expect ionization to be suppressed. Still, appreciable ionization takes place. Inspection of the wavefunction dynamics shows that the electron absorbs energy, when it hits the potential well barrier. The electron collides during each half cycle with the potential barrier and absorbs energy, until its energy is large enough to escape over the barrier. We have dubbed this mechanism laser de-phasing heating (LDH). The strength of LDH scales with the ratio of electron excursion amplitude to well width. Therefore, ionization in figure 5.1 drops to zero for increasing  $L$ .

LDH is a classical process. This follows from a comparison of the quantum result to classical simulations. A set of trajectories, with starting points covering the classically allowed part of the potential well, is launched. The trajectories are weighted with the probability of the ground state wavefunction. The initial velocity is calculated by  $v_i = \pm\sqrt{2(I_p - D)}$ . The classical equations of motion are solved subject to these initial conditions. The ionization probability is determined by the sum over the weight of the trajectories that are free after the laser pulse. The result is depicted by the dotted line in figure 5.1. The agreement with the quantum results is good, proving the classical nature of LDH ionization.

We now turn our attention to the more sophisticated multi-electron case, namely the model of a 4-electron system with Hamiltonian

$$H(x_1, \dots, x_4; t) = \sum_{i=1}^4 \left[ H_1(x_i; t) + \sum_{j>i}^4 \frac{1}{\sqrt{(x_i - x_j)^2 + 1}} \right]. \quad (5.4)$$

Here, the electron-electron interaction is simulated by a non-singular, soft-core Coulomb potential, and  $H_1(x; t)$  denotes the single-particle operator given by equation (5.1) with the parameters set to  $I_p = 0.448$ ,  $L = 100$ ,  $\lambda_0 = 800\text{nm}$ , Gaussian envelope, and FWHM  $\tau = 6\text{fs}$ .

Our analysis shows that ionization by LDH and suppression of tunnel ionization also exists in the multi-electron case. This is corroborated by the excellent agreement between quantum

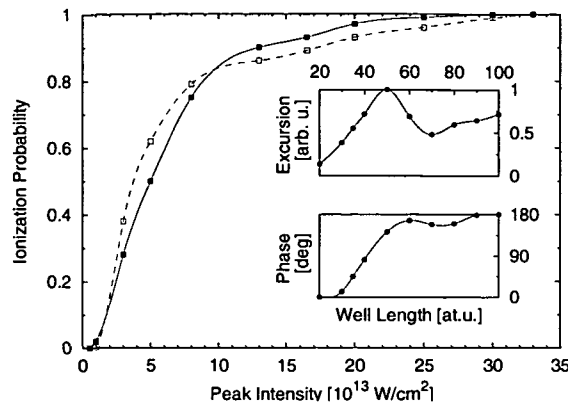


**Figure 5.2.** Quantum mechanical (full squares) and classical (open squares) ionization probability versus laser intensity of a square well potential with 4 electrons ( $I_p = 0.448$ ). The laser parameters are: wavelength  $\lambda_0 = 800\text{nm}$ , and  $\tau_{\text{FWHM}} = 6\text{fs}$  (Gaussian). Inset: normalized excursion of the center of gravity of the electron density at the peak of the laser pulse (upper part), phase relation between laser electric field and the center of gravity motion of the electron density (lower part) versus  $L$  (Intensity,  $I = 5 \times 10^{13}\text{W/cm}^2$ ).

and classical calculations for the 4-electron system depicted in figure 5.2, where we show the ionization probability as a function of laser peak intensity.

In multi-electron systems the transition between under- and over-resonant behavior is more complex than in the single-electron case discussed above, as in addition to single-electron excitations collective effects play a strong role. In unbounded materials the collective response is determined by the plasma frequency  $\omega_p = \sqrt{4\pi\rho_0}$  with  $\rho_0$  the electron density. In finite systems, such as in molecules and in clusters, the resonance frequency is changed by a geometry dependent factor. In our 1D model the resonance is, like in spherical clusters, determined by the plasmon (Mie) frequency,  $\omega_m = \omega_p/\sqrt{3}$ .

The inset of figure 5.2 shows that collective effects dominate over single-electron excitations. We have plotted the normalized excursion amplitude of the center of gravity of the electron density at the peak of the laser pulse (upper part), and the phase relation between laser and electron oscillation (lower part) as a function of  $L$  for  $I = 5 \times 10^{13}\text{W/cm}^2$ . By using  $\rho_0 = (f/L)^3$  with  $f = 4$  we find that  $\omega_m = \omega$  at  $L \approx 40$ . This is in accordance with the position of the resonance in the inset. With decreasing  $b$  the electron motion changes from over-resonant,  $180^\circ$  out of phase to under-resonant, in-phase motion with the laser electric field. This can be understood in terms of the dynamic polarizability,  $\alpha(\omega) = \alpha_0/(\omega_m^2 - \omega^2)$ , with  $\alpha_0$  the static polarizability. For  $\omega \ll \omega_m$  the dynamic polarizability goes over into the static polarizability, whereas for  $\omega \gg \omega_m$  the polarizability changes sign explaining the  $180^\circ$  phase change.

Typical plasma frequencies of large molecules, of clusters, and of condensed matter lie between  $\approx 0.035$  (1eV) and  $\approx 1$  (27.2eV). Therefore, in most of these media the over-resonant limit is not reached. Suppression of tunnel ionization and LDH are important in nano-structures, such as quantum wells and quantum dots, and in semiconductors [72], where electron density and plasma frequency can be tailored by doping. The dependence of the electron dynamics and of ionization on laser wavelength and electron density opens novel ways to control carrier dynamics

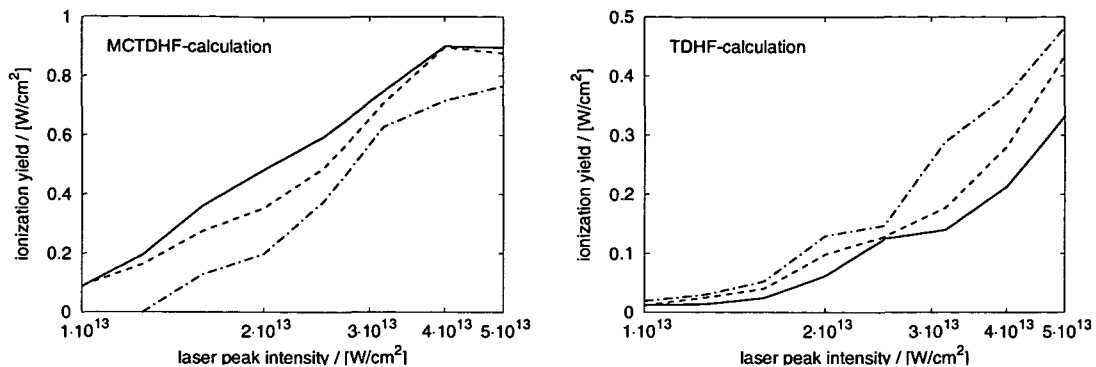


**Figure 5.3.** Ionization (defined as loss of norm within the simulation boundaries) of 2 (full line), 4 (dashed line), and 6 (dashed dotted line) electron molecules ( $I_p = 0.3$ ) by an 800nm laser pulse and duration 10fs FWHM (Gaussian) in a multi-configuration time-dependent Hartree-Fock (left) and a (single configuration) TDHF (right) approach.

in nano-structures.

In the remainder of the chapter we generalize ionization in the under-resonant limit to multi-electron systems. This limit applies to the interaction of infrared laser light with most molecules and clusters. Even in the under-resonant regime, the plasmon frequency plays an important role in ionization. Recently it was suggested that non-adiabatic transitions to excited states can take place [15], resulting in an enhancement of ionization. Our analysis shows that the plasmon resonance plays a dominant role in the non-adiabatic regime of ionization. Here, we focus on the adiabatic limit  $\omega \ll \omega_m$ , where transitions to excited states, such as the plasmon resonance, can be neglected, and  $\alpha(\omega) \approx \alpha_0$ .

Our multi-electron system is described by a model potential consisting of a chain of  $f$  Coulomb nuclei with 1 electron per nucleus. The total, time-independent potential reads

$$V(x_1, \dots, x_f) = \sum_{i=1}^f V_1(x_i) + \sum_{j>i}^f \frac{1}{\sqrt{(x_i - x_j)^2 + a_e}}, \quad (5.5)$$

$$V_1(x) = - \sum_{j=1}^f \frac{1}{\sqrt{(x - jd)^2 + a_n}}, \quad (5.6)$$

with  $d$  the distance between adjacent nuclei. Note that in the asymptotic limit this potential goes over into a Coulomb potential. The laser field is coupled in dipole approximation and velocity gauge. Figure 5.3 shows the dependence of the ionization probability as a function of the intensity for molecules with  $f = 2, 4$ , and 6 centers. The ionization potential for all 3 cases is kept constant,  $I_p = 0.3$ . The remaining parameters are:  $d = 1.4$ ,  $a_e = 1$ ,  $a_n$  is adjusted to keep  $I_p$  constant,  $\lambda = 800\text{nm}$ ,  $\tau_{\text{FWHM}} = 10\text{fs}$ , and a Gaussian pulse shape. In contrast to our discussion of the single electron case, here ionization is reduced for longer molecules. This interesting feature is consistent with recent experimental findings [15, 16]. Note, however, that for identical parameters a single configuration calculation reveals a different picture as can be seen in figure 5.3, too. In contradiction to above mentioned experiments, TDHF predicts an increased ionization probability for larger molecules. As in the previous example of non-sequential double-ionization MCTDHF

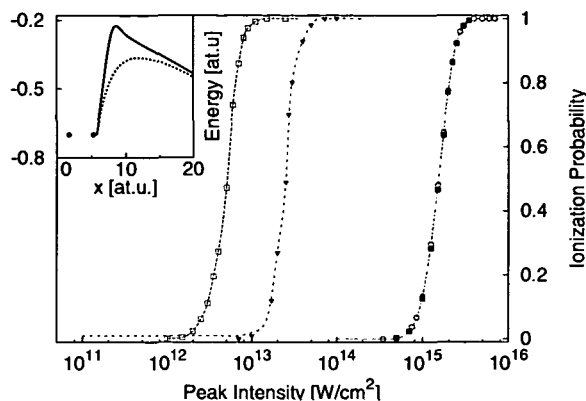


**Figure 5.4.** Ionization probability of the HOMO electron versus laser peak intensity. Full triangles: 4-electron molecule ( $I_p = 0.261$ ); empty squares: corresponding SAE calculation. Full squares: 2-electron He ( $I_p = 0.9$ ); empty circles: He SAE calculation. The laser parameters are: wavelength  $\lambda_0 = 800\text{nm}$ , and  $\tau_{\text{FWHM}} = 6\text{fs}$  (Gaussian). Inset: tunneling barrier in the presence (full) and absence (dotted) of electron polarization.

converges, where TDHF fails qualitatively. This indicates that suppression of ionization is caused by electron correlation, which cannot be taken into account by single-configuration calculations.

In the following the multi-electron effects are identified by a comparison of multi-electron and SAE-electron systems having the same ionization potential. The SAE potential is assumed to be a smoothed Coulomb potential outside the leftmost and rightmost nucleus of the molecule considered below, and constant inside. The well depth is chosen to obtain the same  $I_p = 0.261$  as for the 4-electron molecule, which is modeled by  $d = 3.5$ ,  $a_n = 2.25$ , and  $a_e = 0.81$ . Finally, the laser pulse is Gaussian,  $\lambda_0 = 1500\text{nm}$ , and  $\tau = 10\text{fs}$ .

The comparison of SAE (empty squares) and 4-electron (full triangles) calculations in figure 5.4 reveals that multi-electron effects dominate tunnel ionization. Despite the same ionization potential, the 4-electron saturation intensity of ionization is by a factor of 5 larger than the SAE result. Taking the 1D nature of our analysis and experimental uncertainties into account, this result is in reasonable agreement with measurements, where an increase of the saturation intensity by factors of 3-8, as compared to SAE theory, was obtained [68, 15, 30].

It is interesting to make the same comparison for He. From comparison with experiments it is known that the SAE approximation works well for noble gases. For  $a_e = 0.55$  and  $a_n = 0.55$  the ionization potential of He,  $I_p = 0.9$ , is obtained. The 2 electron (full squares) and the SAE (empty circles) calculation in figure 5.4 coincide, giving the first proof of the validity of the SAE approximation.

Finally, the physical origin of the violation of the SAE approximation in complex systems needs to be identified. In the single electron case we have seen that the electron is pushed against the tunnel barrier by the laser field. In the multi-electron case the same process polarizes the molecule. The resulting modification of the molecular potential results in an increase of the tunneling barrier, as is shown in the inset of figure 5.4. The inset shows the potential of nuclei, remaining bound electrons, and laser field as felt by the tunneling electron (full line) at the peak of the laser pulse, where the polarization is maximum. The dotted potential is calculated from

the field free 4-electron wavefunction, where the molecule's polarization is zero. Comparison of the two curves reveals a polarization caused increase of the molecular tunneling barrier.

Our analysis revealed the key parameters determining ionization of complex systems, which are, size, geometry, and polarizability. It showed that in particular the increased polarizability makes ionization of complex materials fundamentally different from noble gas atoms. The ratio of laser frequency,  $\omega$ , to the resonance frequency,  $\omega_m$ , of collective electron motion determines the dynamic polarizability and therewith the response of the electrons to the laser field. We identified two distinct ionization mechanisms in the over- ( $\omega \gg \omega_m$ ) and under-resonant regime ( $\omega \ll \omega_m$ ).

In the over-resonant limit the electrons move  $180^\circ$  out of phase with the laser field, and therewith away from the tunneling barrier. As a result, tunnel ionization is suppressed and classical over-the-barrier ionization becomes dominant. In the under-resonant limit the electrons are pushed towards the tunneling barrier, creating a polarization that increases the tunneling barrier and reduces ionization in agreement with the reduction of ionization observed in large molecules [15, 30, 68].

## Chapter 6

---

### Conclusions

We have studied multi-electron ionization in molecules in a non-perturbative, strong field regime. To investigate the laser-molecule interaction we have applied two different, time-dependent approaches. Both methods permit to consider non-linear excitation dynamics of multi-particle systems and the role of inter-electron correlations in strong-field ionization.

In particular we have analyzed shake-up excitation in Deuterium theoretically as well as experimentally. Our theoretical analysis is performed in two steps:

- (i) an electron ionizes via tunneling described by the quasi-static molecular ADK-theory.
- (ii) after the electron is born in the continuum the interaction of the electrons is calculated using a time-dependent Keldysh-type method.

This analytical model excellently agrees with experiments. We found that shake-up produces one excited  $\sigma_u D_2^+$  state per  $10^5$  ionization events. Our theory predicts the shake-up mechanism to be efficient for large molecules, where the energy spacing between the levels becomes small.

However, the method summarized above is particularly tailored to model shake-up. Its general scope of application is essentially restricted to the description of two active electrons. To overcome this limit we have introduced the multi-configuration time-dependent Hartree-Fock (MCTDHF) method.

MCTDHF is a numerical efficient approach to solve the time-dependent Schrödinger equation. In contrast to time-dependent Hartree-Fock, here the exact wave function is expanded in several Slater determinants. Thus increasing its accuracy while remaining computationally feasible.

We have tested our approach on highly correlated two electron systems and demonstrated that by systematic inclusion of correlation the MCTDHF method provides a good approximation of time-dependent multi-electron wave functions. For bound states dynamics MCTDHF provides a rapidly convergent expansion. For ionizing systems MCTDHF is capable of describing the strongly correlated process of double ionization correctly. A quantitative description of single and double ionization within an accuracy of 5% can be achieved with reasonable number of configurations. We have detected no artefacts of the method.

From a computational point of view, the key property of the method is the favorable scaling behavior when compared to straight-forward discretization of a multi-electron system. Whereas the number of points in straight forward discretization grows exponentially with the number of particles  $f$ , MCTDHF scales linearly  $\propto n \geq f$  for the factor functions  $\varphi$ . The demonstrated convergence behavior and moderate increase of problem size with the number of electrons makes MCTDHF a powerful approach for the calculation of the correlated dynamics of many-electron

systems in strong fields, where calculations with up to 10 active electrons and a significant amount of correlation may be feasible.

The present demonstration of the MCTDHF method is only in 1D. The main challenge for extending the method to 3D is finding a discretization of the 3D factor functions  $\varphi(\vec{x})$ , which allows efficient computation of 3D and 6D integrals. This is currently a main research topic of our group. However, it is important to notice that the extension to 3D, in principle, only affects the factor functions, whereas the scaling behavior with respect to  $f$  and  $n$  is independent of dimensionality.

We have applied MCTDHF to study ionization of (model) 1D multi-electron systems. Our analysis shows that ionization in complex systems is radically different from noble gas atoms. Ionization in molecules is governed by four key parameters, that are size, geometry, electron mobility, and polarizability. In particular the polarizability adds a correlated multi-electron component to tunnel ionization, which depends strongly on the ratio of the laser frequency to the frequency of collective electron motion. Despite the 1D nature of our calculations reasonable agreement with experiments shows that the essential effects of tunnel ionization can be captured by a 1D analysis.

## References

---

- [1] E. Deumens, A. Diz, R. Longo, and Y. Öhrn. Time-dependent theoretical treatments of the dynamics of electrons and nuclei in molecular systems. *Rev. Mod. Phys.*, 66(3):917, July 1994.
- [2] M. Drescher et al. Time-resolved atomic inner-shell spectroscopy. *Nature*, 419(6909):803, October 2002.
- [3] J. Karczmarek, J. Wright, P. Corkum, and Misha Ivanov. Optical centrifuge for molecules. *Phys. Rev. Lett.*, 82(17):3420, April 1999.
- [4] M. Hentschel et al. Attosecond metrology. *Nature*, 414(6863):509, November 2001.
- [5] H. Niikura et al. Sub-laser-cycle electron pulses for probing molecular dynamics. *Nature*, 417(6892):917, June 2002.
- [6] R. Kienberger et al. Atomic transient recorder. *Nature*, 427(6977):817, February 2004.
- [7] A.D. Bandrauk and H.-Z. Lu. Numerical methods for molecular time-dependent Schrödinger equations - bridging the perturbative to non-perturbative regime. In C. Le Bris, P.G. Ciarlet, and J.L. Lions, editors, *Handbook of numerical analysis Volume X: Special Volume: Computational Chemistry*, chapter 13, page 803. Elsevier Sciences, Amsterdam, April 2003.
- [8] J. Parker, L. Moore, D. Dundas, and K. Taylor. Double ionization of helium at 390 nm. *J. Phys. B: At. Mol. Opt. Phys.*, 33(20):L691, October 2000.
- [9] P. G. Burke and V. M. Burke. Time-dependent R-matrix theory of multiphoton processes. *J. Phys. B: At. Mol. Opt. Phys.*, 30(11):L383, June 1997.
- [10] J. Zhang and P. Lambropoulos. Non-perturbative time-dependent theory and ATI in two electron atoms. *J. Phys. B: At. Mol. Opt. Phys.*, 28(7):L101, March 1995.
- [11] K. J. Schafer, B. Yang, L. F. DiMauro, and K. C. Kulander. Above threshold ionization beyond the high harmonic cutoff. *Phys. Rev. Lett.*, 70(11):1599, March 1993.
- [12] K. C. Kulander. Multiphoton ionization of hydrogen: A time-dependent theory. *Phys. Rev. A*, 35(1):445, January 1987.
- [13] M. V. Ammosov, N. B. Delone, and V. P. Krainov. Tunnel ionization of complex atoms and of atomic ions in an alternating electromagnetic field. *Sov. Phys. - JETP*, 64:1191, 1986.
- [14] X. M. Tong, Z. X. Zhao, and C. D. Lin. Theory of molecular tunneling ionization. *Phys. Rev. A*, 66:033402, September 2002.
- [15] M. Lezius, V. Blanchet, M. Ivanov, and A. Stolow. Polyatomic molecules in strong laser fields: Nonadiabatic multielectron dynamics. *J. Chem. Phys.*, 117(4):1575, July 2002.
- [16] M. Lezius et al. Nonadiabatic multielectron dynamics in strong field molecular ionization. *Phys. Rev. Lett.*, 86(1):51, January 2001.
- [17] V. Schmidt. *Electron Spectrometry of Atoms using Synchrotron Radiation*. Cambridge University Press, Cambridge, U.K., 1997.
- [18] D. N. Fittinghoff, P. R. Bolton, B. Chang, and K. C. Kulander. Observation of nonsequential double ionization of helium with optical tunneling. *Phys. Rev. Lett.*, 69(18):2642, November 1992.
- [19] P. B. Corkum. Plasma perspective on strong-field multiphoton ionization. *Phys. Rev. Lett.*, 71(13):1994, September 1993.
- [20] J. H. McGuire et al. The ratio of cross sections for double to single ionization of helium by high energy photons and charged particles. *J. Phys. B*, 28(6):913, March 1995.

- [21] L.V. Keldysh. *Zh. Eksp. Teor. Fiz.*, 47:1945, 1964.
- [22] E. Runge and E. K. U. Gross. Density-functional theory for time-dependent systems. *Phys. Rev. Lett.*, 52(12):997, March 1984.
- [23] D. Bauer. Two-dimensional, two-electron model atom in a laser pulse: Exact treatment, single-active-electron analysis, time-dependent density-functional theory, classical calculations, and non-sequential ionization. *Phys. Rev. A*, 56(4):3028, October 1997.
- [24] K. C. Kulander. Time-dependent Hartree-Fock theory of multiphoton ionization: Helium. *Phys. Rev. A*, 36(6):2726, September 1987.
- [25] K. C. Kulander. Time-dependent theory of multiphoton ionization of xenon. *Phys. Rev. A*, 38(2):778, January 1988.
- [26] M. S. Pindzola, D. C. Griffin, and C. Bottcher. Validity of time-dependent Hartree-Fock theory for the multiphoton ionization of atoms. *Phys. Rev. Lett.*, 66(18):2305, May 1991.
- [27] M. S. Pindzola, T. W. Gorczyca, and C. Bottcher. Two-photon ionization of lithium in the time-dependent Hartree-Fock approximation. *Phys. Rev. A*, 47(6):4982, June 1993.
- [28] M. S. Pindzola, P. Gavras, and T. W. Gorczyca. Time-dependent unrestricted Hartree-Fock theory for the multiphoton ionization of atoms. *Phys. Rev. A*, 51(5):3999, May 1995.
- [29] M. S. Pindzola, F. Robicheaux, and P. Gavras. Double multiphoton ionization of a model atom. *Phys. Rev. A*, 2:1307, February 1997.
- [30] V. R. Bhardwaj, P. B. Corkum, and D. M. Rayner. Internal laser-induced dipole force at work in C<sub>60</sub> molecule. *Phys. Rev. Lett.*, 91(20):203004, November 2003.
- [31] M. Smits, C. A. de Lange, A. Stolow, and D. M. Rayner. Dynamic polarization in strong field ionization of small metal clusters. *Phys. Rev. Lett.*, 2004. submitted.
- [32] V. Veniard, R. Taieb, and A. Maquet. Photoionization of atoms using time-dependent density functional theory. *Laser Physics*, 13(4):465, 2003.
- [33] P. Dietrich, N.H. Burnett, M. Ivanov, and P.B. Corkum. High-harmonic generation and correlated two-electron multiphoton ionization with elliptically polarized light. *Phys. Rev. A*, 50(5):R3585, November 1994.
- [34] A. Kornev, E. B. Tulenko, and B. A. Zon. Kinetics of multiple ionization of rare-gas atoms in a circularly polarized laser field. *Phys. Rev. A*, 68:043414, October 2003.
- [35] Ch. Fabian, M. Kitzler, N. Milosevic, and T. Brabec. Multi-electron strong field theory. *J. Mod. Optics*, 50(3-4):589, February 2003.
- [36] A. Becker and F. H. M. Faisal. S-matrix analysis of coincident measurement of two-electron energy distribution for double ionization of He in an intense laser field. *Phys. Rev. Lett.*, 89(October):193003, 2002.
- [37] M. Lewenstein et al. Theory of high-harmonic generation by low-frequency laser fields. *Phys. Rev. A*, 49(3):2117, March 1994.
- [38] P. W. Atkins and R. S. Friedman. *Molecular Quantum Mechanics*. Oxford University Press Inc., New York, third edition edition, 1997.
- [39] K. Codling, L. J. Frasinski, and P. A. Hatherly. On the field ionisation of diatomic molecules by intense laser fields. *J. Phys. B*, 22(12):L321, June 1989.
- [40] T. Seideman, M. Yu. Ivanov, and P. B. Corkum. Role of electron localization in intense-field molecular ionization. *Phys. Rev. Lett.*, 75:2819, 1995.
- [41] I.V. Litvinyuk et al. Alignment-dependent strong field ionization of molecules. *Phys. Rev. Lett.*, 90:233003, June 2003.
- [42] A. Zavriyev, P. H. Bucksbaum, H.G. Muller, and D. W. Schumacher. Ionization and dissociation of H<sub>2</sub> in intense laser fields at 1.064  $\mu\text{m}$ , 532 nm, and 355 nm. *Phys. Rev. A*, 42(9):5500, November 1990.
- [43] F. Châteauneuf, T.-T. Nguyen-Dang, N. Ouellet, and O. Atabek. Dynamical quenching of field-induced dissociation of H<sub>2</sub><sup>+</sup> in intense infrared lasers. *J. Chem. Phys.*, 108(10):3974, March 1998.
- [44] Ionization data courtesy of X. M. Tong and C. D. Lin.
- [45] M. H. Beck, A. Jäckle, G. A. Worth, and H.-D. Meyer. The multiconfiguration time-dependent hartree (MCTDH) method: A highly efficient algorithm for propagating wavepackets. *Physics*

- Report*, 324(1):1, January 2000.
- [46] P. A. M. Dirac. *Proc. Cambridge Philos. Soc.*, 26:376, 1930.
  - [47] J. Frenkel. *Wave Mechanics*. Clarendon Press, Oxford, 1934.
  - [48] C. Lubich. A variational splitting integrator for quantum molecular dynamics. *App. Num. Math.*, 48(3):355, March 2004.
  - [49] O. Koch, W. Kreuzer, and A. Scrinzi. MCTDHF in ultrafast laser dynamics. AURORA TR2003-29. Available at <http://www.vcpc.univie.ac.at/aurora/publications/>, 2003.
  - [50] H.-D. Meyer and G. A. Worth. Quantum molecular dynamics: Propagating wavepackets and density operators using the multi-configuration time-dependent Hartree (MCTDH) method. *Theor. Chem. Acc.*, 109(5):251, June 2003.
  - [51] H. Wang and M. Thoss. Multilayer formulation of the multiconfiguration time-dependent Hartree theory. *J. Chem. Phys.*, 119(3):1289, July 2003.
  - [52] J. Caillat et al. Correlated multielectron systems in strong laser pulses - an MCTDHF approach. *Phys. Rev. A*, 2004. submitted.
  - [53] Th. Mercouris, Y. Komninos, S. Dionissopoulou, and C. A. Nicolaides. Computation of strong-field multiphoton processes in polyelectronic atoms: State-specific method and applications to H and  $\text{Li}^-$ . *Phys. Rev. A*, 50(5):4109, November 1994.
  - [54] K. C. Kulander, K. J. Shafer, and J. L. Krause. In M. Gavrilu, editor, *Atoms in Intense Laser Fields*, page 247. Academic Press Inc. London, 1992.
  - [55] K. Blum. *Density Matrix Theory and Applications*. Plenum Press, New York, 2nd edition, 1996.
  - [56] P.-O. Löwdin. Quantum theory of many-particle systems. I. Physical interpretations by means of density matrices, natural spin-orbitals, and convergence problems in the method of configurational interaction. *Phys. Rev.*, 97(6):1474, March 1955.
  - [57] U. Manthe. Comment on "A multiconfiguration time-dependent Hartree approximation based on natural single-particle states" [*J. Chem. Phys.* 99, 4055 (1993)]. *J. Chem. Phys.*, 101(3):2652, August 1994.
  - [58] M. W. Schmidt and M. S. Gordon. The construction and interpretation of MCSCF wavefunctions. *Annu. Rev. Phys. Chem.*, 49(1):233, 1998.
  - [59] C. Leforestier and R. E. Wyatt. Optical potential for laser induced dissociation. *J. Chem. Phys.*, 78(5):2334, March 1983.
  - [60] Q. Su and J. H. Eberly. Model atom for multiphoton physics. *Phys. Rev. A*, 44(9):5997, November 1991.
  - [61] E. Schmidt. Zur Theorie der linearen und nichtlinearen Integralgleichungen. I Teil. *Mathematische Annalen*, page 433, 1907.
  - [62] U. Schwengelbeck. Analytical solution of the Schrödinger equation of a laser-driven two-particle system. *Phys. Lett. A*, 253(3-4):168, March 1999.
  - [63] R. Grobe, K. Rzazewski, and J. H. Eberly. Measure of electron-electron correlation in atomic physics. *J. Phys. B: At. Mol. Opt. Phys.*, 27(16):L503, August 1994.
  - [64] R. Grobe and J. H. Eberly. Double multiphoton ionization of a model atom. *Phys. Rev. A*, 55(2):1307, February 1997.
  - [65] L. V. Keldysh. Ionization in the field of a strong electromagnetic wave. *Sov. Phys. - JETP*, 20:1307, 1965.
  - [66] C. Guo. Multielectron effects on single-electron strong field ionization. *Phys. Rev. Lett.*, 85(11):2276, September 2000.
  - [67] B. Walker et al. Precision measurement of strong field double ionization of helium. *Phys. Rev. Lett.*, 73(9):1227, August 1994.
  - [68] S. M. Hankin, D. M. Villeneuve, P. B. Corkum, and D. M. Rayner. Nonlinear ionization of organic molecules in high intensity laser fields. *Phys. Rev. Lett.*, 84(22):5082, May 2000.
  - [69] A. N. Markevitch et al. Nonadiabatic dynamics of polyatomic molecules and ions in strong laser fields. *Phys. Rev. A*, 68:011402(R), July 2003.
  - [70] M. J. DeWitt and R. J. Levis. Observing the transition from a multiphoton-dominated to a field-mediated ionization process for polyatomic molecules in intense laser fields. *Phys. Rev. Lett.*,

81(23):5101, December 1998.

- [71] L. D. Landau and E. M. Lifshitz. *Mechanics*. Pergamon Press, Oxford, New York, 1976.
- [72] L. Jacak, P. Hawrylak, and A. Wojs. *Quantum Dots*. Springer-Verlag, Berlin, 1998.

**EUROPEAN  
CURRICULUM VITAE  
FORMAT**



**PERSONAL INFORMATION**

Name	<b>Jürgen ZANGHELLINI</b>
Address	<b>Reschgasse 5/18, A-1120 Wien, Austria, EU</b>
Telephone	<b>+43-1-817 94 82</b>
Email	juergen.zanghellini@tuwien.ac.at
Nationality	Austrian
Date of birth	25.04.1976

**WORK EXPERIENCE**

- Dates (from-to) May 2001 – present
- Name and address of employer Photonics Institute, Vienna University of Technology  
Gußhausstraße 27/387, A-1040 Wien, Austria, EU
- Occupation or position held Ph.D. student
- Dates (from-to) September 2002 – September 2004
- Name and address of employer University of Ottawa, Faculty of Science, Physics  
150 Louis Pasteur St., Ottawa, ON, K1N 6N5 Canada
- Occupation or position held Research Associate

**EDUCATION AND TRAINING**

- Dates (from-to) May 2001 – present
- Name and type of organization providing education and training Vienna University of Technology, Austria
- Principal subjects Faculty of Electrical Engineering and Information Technology  
Ph.D. student, theoretical physics
- Dates (from-to) 1995 – April 2001
- Name and type of organization providing education and training Vienna University of Technology, Austria
- Principal subjects Faculty of Electrical Engineering and Information Technology  
Automation Technology
- Title of qualification awarded *Dipl.-Ing.* (MSc) in electrical engineering
- Dates (from-to) 1990 – 1995
- Name and type of organization providing education and training HTL Waidhofen/Ybbs, Austria
- Principal subjects Electrical engineering
- Title of qualification awarded *Matura* (school leaving examination)

## ADDITIONAL INFORMATION

### PUBLICATIONS

A. Pegarkov, J. Zanghellini, Ch. Jungreuthmayer, and T. Brabec.

*Ionization dynamics of multi-electron systems in strong laser pulses,*

chapter for *Focus on Laser and Electro-Optics Research*, edited by W. Arkin (Nova Science Publishers, to be published 2005).

J. Zanghellini, Ch. Jungreuthmayer, A. Pegarkov, and T. Brabec.

*Plasmon signatures in high harmonic generation,*

submitted to *Phys. Rev. Lett.* (2004).

J. Caillat, J. Zanghellini, M. Kitzler, W. Kreuzer, O. Koch, and A. Scrinzi.

*Correlated multi-electron systems in strong laser pulses - an MCTDHF approach,*

submitted to *Phys. Rev. A*, (2004).

I. Litvinyuk, I. Litvinyuk, F. Légaré, P. W. Dooley, D. M. Villeneuve, and P. B. Corkum (experiments), J. Zanghellini, A. Pegarkov, C. Fabian, and T. Brabec (theory).

*Shake-up excitation during intense field tunnel ionization,*

submitted to *Phys. Rev. Lett.* (2004).

J. Zanghellini, M. Kitzler, Z. Zhang, and T. Brabec.

*Multi-electron dynamics in strong laser fields,*

submitted to *J. Mod. Opt.* (2004), accepted.

M. Kitzler, J. Zanghellini, Ch. Jungreuthmayer, M. Smits, A. Scrinzi, and T. Brabec.

*Ionization dynamics of extended multi-electron systems,*

*Phys. Rev. A* **70**, Rapid Communications, 041401(R) (2004)

Ch. Jungreuthmayer, M. Geissler, J. Zanghellini, and T. Brabec.

*Microscopic Analysis of Large-Cluster Explosion in Intense Laser Fields,*

*Phys. Rev. Lett.* **92**, 133401 (2004).

J. Zanghellini, M. Kitzler, T. Brabec, and A. Scrinzi.

*Testing the time-dependent Hartree-Fock method,*

*J. Phys. B* **37**, 763 (2004).

J. Zanghellini, M. Kitzler, Ch. Fabian T. Brabec, and A. Scrinzi.

*A MCTDHF approach to multi-electron dynamics in laser fields,*

*Laser Physics* **13**, 1064 (2003).